

Community composition of epipelagic zooplankton in the Eurasian
Basin 2017 determined by ZooScan image analysis

von

Julian Koplin

geboren am

05.07.1994

Bachelorarbeit

im Studiengang Bachelor of Science Biologie

der Universität Hamburg

25.04.2020

Erstgutachter: Dr. Jens Floeter

Zweitgutachter: Dr. Hauke Flores

Table of Contents

1 Introduction	1
2 Material and Methods.....	6
2.1 Sampling.....	6
2.2 Sample analysis	8
2.3 ZooScan image analysis	9
2.4 Abundance, Biovolume and Biomass	10
2.5 Statistical analysis	13
3 Results	14
3.1 Description of the taxa, community composition and taxa abundance.....	14
3.2 Copepods.....	18
3.3 Selected copepod taxa	20
3.3.1 <i>Calanus finmarchicus/glacialis</i>	20
3.3.2 <i>Calanus hyperboreus</i>	21
3.3.3 <i>Metridia longa</i>	22
3.4 Non-copepod taxa.....	23
3.5 Biovolume and Biomass.....	25
3.6 Composition of size-fractions	29
3.7 Comparison of Abundance, Biovolume and Biomass.....	32
3.8 Comparison of ZooScan-based biomass and dry weight biomass	33
4 Discussion	36
5 Literature	44
6 Appendix	52
7 Acknowledgements	57
Declaration of academic honesty	57

Table of Figures

Figure 1: Bathymetric map of the Arctic Ocean, the red arrows showing general circulation and the bigger arrows the importance of riverine inflow. From Michel et al. (2012), adapted from Carmack (2000) and Jakobsson et al. (2004, 2008).	3
Figure 2: Overview of the RMT stations during the Polarstern expedition PS106.2.....	6
Figure 3: Water masses of upper 400 m at all station, hydrographic information by A. Nikolopoulos (unpublished data)	8
Figure 4: Results of cluster analysis of 15 stations (samples), analysis based on Bray Curtis similarity. With cluster numbers 1 and 2.	14
Figure 5: Taxonomic composition at all stations. Abundances (left panel) and relative abundances (right panel). Copepoda with a contribution < 4% are grouped as “Other Copepoda” and non-copepod taxa with contribution <1% are grouped as “Other Taxa.	17
Figure 6: Species composition of copepods at all stations. Abundances (left panel) and relative abundances (right panel). Copepods with contribution <4% were grouped as “Other Copepoda”, Calanoida with contribution <3% were grouped as “Other Calanoida”.	20
Figure 7: Developmental stage composition of <i>Calanus finmarchicus/glacialis</i> at all stations. Abundances (left panel) and relative abundances (right panel).	21
Figure 8: Stage composition of <i>Calanus hyperboreus</i> at all stations. Abundances (left panel) and relative abundances (right panel).....	22
Figure 9: Stage composition of <i>Metridia longa</i> at all stations. Abundances (left panel) and contribution (right panel).....	23
Figure 10: Species composition of non-copepods at all stations. Abundances (left panel) and relative abundance (right panel). Taxa with contribution <0.05% were grouped as “Other Taxa”	24
Figure 11: Biovolume in mm ³ m ⁻³ at all stations (left panel) and biovolume contribution at all stations (right panel). Split in size-fractions.....	26

Figure 12: Relationship between ZooScan-based biovolume and biomass converted from the biovolume, with linear trend-line. There is a significant positive relationship. Linear regression: $y = 11.74x + 46.574$ $R^2 = 0.81$, $p < 0.001$) 26

Figure 13: Total biomass (mg m^{-3}) of all 15 stations, split by cluster. Median values marked as red crosses (x). 28

Figure 14: Biomass in mg m^{-3} at all stations (left panel) and biomass contribution at all stations (right panel). Split in size-fractions..... 28

Figure 15: Total biomass in mg m^{-3} for all size-fractions (left panel) and biomass contribution for all size-fractions in % (right panel). 29

Figure 16: Total biomass contribution (%) of Copepoda taxa, split in size-fractions..... 31

Figure 17: Relationship between biomass and abundance, with linear trend-line. There is a significant positive relationship. Linear regression: $y = 8.0109x - 13.072$ $R^2 = 0.89$, $p < 0.001$)..... 32

Figure 18: Relationship between biovolume and abundance, with linear trend-line. There is a significant positive relationship. Linear regression: $y = 0.5288x - 23.282$ $R^2 = 0.66$, ($p < 0.001$) 32

Figure 19: Relationship between ZooScan-based biomass and dry weight measured biomass, with linear trend-line. Blue line indicates 1:1 relationship. There is a significant positive relationship. Linear regression: $y = 0.3714x + 1.3301$ ($R^2 = 0.573$, $p = 0.004$)..... 33

Figure 20: Accumulated biomass of all stations, split in size-fractions..... 35

Figure 21: Exemplary relationship between ZooScan-based biomass and dry weight measured biomass with trendline, for the size-fractions 500-1000 μm (gray), 1000-2000 μm (yellow) and 2000-4000 μm (blue)..... 35

Figures in Appendix

Figure A. 1: Confusion matrix from EcoTaxa, diagonal contains the recall rate, darker blue indicates a higher rate. For all categories see Tab. A.3..... 55

Figure A. 2: Confusion matrix from EcoTaxa, diagonal contains the precision rate, darker blue indicates a higher rate. For all categories see Tab. A.3..... 55

List of Tables

Table 1: Summary of RMT hauls conducted during PS106/2	7
Table 2: Reg. and corr. parameters obtained from Lehette and Hernandez-Leon (2009).....	12
Table 3: Total number of taxa and combined abundance of all taxa at the sampling sites. Split in size-fractions.	15
Table 4: Abundance of all Copepods at the sampling sites. Split in size-fractions.	16
Table 5: Abundance of all taxa within different size-fractions, both Clusters and overall in ind. m ⁻³ , median, 25%, 75% quantile (Q.) and average with standard deviation.....	16
Table 6: Shannon-Wiener Index and Evenness of all stations	17
Table 7: Abundance of copepods at all stations, median, quartile (Q.) and average (Avr.) with standard deviation (SD) of all taxa in ind. m ⁻³ ,	18
Table 8: Total relative abundance of copepods at each station in %	19
Table 9: Abundance of non-copepods at all stations, median, quartile (Q.) and average (Avr.) with standard deviation (SD) of all taxa in ind. m ⁻³ ,	25
Table 10: Contribution of size-fractions for zooplankton biomass and biovolume in %.....	27
Table 11: Contribution over all stations for zooplankton biomass and biovolume in %	27
Table 12: Total biomass of taxa, median, quartile (Q.) and average (Avr.) with standard deviation (SD) of all taxa in mg m ⁻³ , split in size-fractions.	30
Table 13: Total biomass contribution of taxa in %, split in size-fractions.....	30
Table 14: Total biomass of Copepoda (mg m ⁻³), split in size-fractions.....	31
Table 15: Total biomass contribution of Copepods (%), split in size-fractions.....	31
Table 16: Total relative contribution of biomass and abundance in %, split in size-fractions.	33
Table 17: Comparison of biomass values between biomass measured by dry weight and ZooScan-based biomass, median, quartile (Q.) and average (Avr.) with standard deviation (SD) in mg m ⁻³	34

Tables in Appendix

Table A. 1: Taxonomic composition and abundance of mesozooplankton across the Barents Sea shelf slope and Nansen Basin for the Atlantic regime Cluster (AR).....	52
Table A. 2: Taxonomic composition and abundance of mesozooplankton across the Barents Sea shelf slope and Nansen Basin for the polar regime Cluster (PR).....	53
Table A. 3: Summary of statistical evaluation (n = sample size, W = Wilcoxon statistical criterion, p-value)	54
Table A. 4: All categories of the learning set in EcoTaxa	56

Abbreviations

AR	Atlantic regime
Avr	Average
AW	Atlantic Water
AWI	Alfred Wegener Institute
C.	<i>Calanus</i>
H	Diversity index of Shannon Wiener
MAW	Modified Atlantic Water
PR	Polar regime
PSW	Polar Surface Water
Q.	Quartile
RMT	Rectangular Midwater Trawl
SD	Standard deviation
wPSW	warm Polar Surface Water

Summary

The Arctic Ocean is especially vulnerable to the impacts of climate change. Warmer ocean temperatures and reduced sea ice coverage lead to a poleward shift of communities in the Arctic Ocean. This process, termed borealization, is considerably changing Arctic marine food web structure with implications for ecosystems dynamics and functioning. Zooplankton is a good indicator of climate change in the marine environment and helps understand what role aberrations in the water mass circulations could play for ecosystem functioning.

To better understand how the communities adapt to the changing environment and what the potential impacts, such as borealization, could mean for the arctic habitats, monitoring the community composition on a regular basis is crucial. Traditional taxonomical analyses are time consuming while the semi-automatic image analysis using ZooScan was developed to reduce time.

This study aims to provide further information on the composition of epipelagic zooplankton communities in the Arctic Ocean determined by ZooScan image analysis and to verify whether there is a biogeographical and hydrographical pattern on the shelf and slope of the Barents Sea and in the Nansen Basin. Additionally, this study tried to confirm whether the taxonomy-based optical method ZooScan leads to similar results as dry-weight measured biomass data in term of size distribution and total biomass in different size fractions.

The expedition PS 106.2 with the research vessel *Polarstern* provided an opportunity to sample the epipelagic zooplankton community from the shelf of the Barents Sea into the Nansen Basin proper, crossing a gradient of decreasing influence of Atlantic Water (AW).

This study confirmed the hypothesis that there was a biogeographical and more importantly hydrographical pattern of mesozooplankton community structure in the study area of PS106. The basin domain is characterized by two basic water masses. The Atlantic regime (AR) with near-surface Atlantic Water (AW) and the polar regime (PR) with AW at a greater depth, overlain with polar surface water and intermediate water. Biomass and abundance were highest along stations in the AR and lowest at stations in the PR. Smaller fractions with high abundances dominated the AR and bigger fractions the PR respectively. In warming Arctic Ocean, growing AW influences can therefore have consequences for the ecosystem structure and the sustainability for marine resources, such as commercially used fish and the characteristic megafauna.

Calanus glacialis and the boreal species *Calanus finmarchicus* were found dominant in the AR. In contrast *Calanus hyperboreus* and *Metridia longa* dominated the PR. This study showed that a more traditional method for calculating biomass such as a dry weight measurement leads to similar relative proportions as ZooScan-based biomass. This would allow for a more rapid taxonomic analysis and biomass calculation of the vast number of samples. However, a correct parametrization of the conversion from 2-dimensional objects on ZooScan pictures to dry mass is critical for an accurate determination of dry weight. Finally, there was a link between high biomasses and high abundances, which could enable faster predictions based on biomass alone in well-studied ecosystems.

Zusammenfassung

Der Arktische Ozean ist besonders anfällig für die Auswirkungen des Klimawandels. Wärmere Meerestemperaturen und eine verringerte Meereisbedeckung führen zu einer polwärts Verschiebung von Gemeinschaften im arktischen Ozean. Dieser als Borealisierung bezeichnete Prozess verändert die Struktur des arktischen marinen Nahrungsnetzes erheblich und hat Auswirkungen auf die Dynamik und Funktionsweise der Ökosysteme. Zooplankton ist ein guter Indikator für Klimaveränderungen in der Meeresumwelt und hilft zu verstehen, welche Rolle Veränderungen der Wassermassenzirkulation für das Funktionieren arktischer Ökosysteme spielen könnten.

Um besser zu verstehen, wie sich die arktischen Gemeinschaften an das sich ändernde Umfeld anpassen und welche potenziellen Auswirkungen Veränderungen wie die Borealisierung auf die arktischen Lebensräume haben könnten, ist eine regelmäßige Erfassung der Zusammensetzung der Zooplanktongemeinschaften von entscheidender Bedeutung.

Herkömmliche taxonomische Analysen sind zeitaufwändig, jedoch wurde mit der halbautomatischen Bildanalyse mit dem ZooScan ein Verfahren entwickelt, das schneller zu Ergebnissen führt.

Diese Studie soll weitere Informationen über die Zusammensetzung der epipelagischen Zooplanktongemeinschaften im Arktischen Ozean liefern, die durch die ZooScan-Bildanalyse ermittelt wurden. Außerdem sollte überprüft werden, ob im Schelf und am Hang der Barentssee sowie im Nansen-Becken ein biogeografisches und hydrographisches Muster vorliegt. Darüber hinaus wurde in dieser Studie versucht zu bestätigen, ob die taxonomiebasierte optische Methode ZooScan zu ähnlichen Ergebnissen führt wie die gemessenen Trockenmasse-Biomassedaten hinsichtlich Größenverteilung und Gesamtbiomasse.

Die Expedition PS 106.2 mit dem Forschungsschiff *Polarstern* bot die Gelegenheit, die epipelagische Zooplanktongemeinschaft vom Schelf der Barentssee bis in das eigentliche Nansen-Becken zu untersuchen und dabei einen Gradienten mit abnehmendem Einfluss von Atlantischen Wasser (AW) zu überqueren.

Diese Studie bestätigte die Hypothese, dass es im Untersuchungsgebiet von PS106 ein biogeografisches und vor allem hydrographisches Muster der Mesozooplanktongemeinschaft gibt. Die Beckendomäne ist gekennzeichnet durch zwei Grundwassermassen. Das atlantische Regime (AR) mit oberflächennahen AW und das polare Regime (PR) mit AW in größerer Tiefe, das von polarem Oberflächen- und Zwischenwasser überlagert wird. Biomasse und Abundanzen waren an Stationen im AR am höchsten und an Stationen im PR am niedrigsten.

Kleinere Fraktionen mit hoher Abundanz dominierten das atlantische Regime und größere Fraktionen das PR. Wachsende AW-Einflüsse könnten daher Konsequenzen für die Ökosystemstruktur und die Nachhaltigkeit von Meeresressourcen bedeuten. *Calanus glacialis* und die boreale Art *Calanus finmarchicus* waren im AR dominant während *Calanus hyperboreus* und *Metridia longa* das PR dominierten. Es wurde gezeigt, dass eine traditionellere Methode zur Berechnung von Biomasse, wie Trockengewichtsmessung, zu ähnlichen relativen Ergebnissen führt wie Biomassebestimmung durch ZooScan, was eine schnellere taxonomische Analyse und Biomasseberechnung der großen Anzahl von Proben ermöglichen würde. Allerdings zeigte sich, dass eine korrekte Parametrisierung der Konversion von flächenbasierten ZooScan-Aufnahmen auf die Trockenmasse kritisch für eine akkurate Ableitung der Trockenmasse ist. Schließlich bestand ein Zusammenhang zwischen hoher Biomasse und hoher Abundanz, was schnellere Vorhersagen auf der Grundlage von Biomasse allein in gut untersuchten Ökosystemen ermöglichen könnte.

1 Introduction

In most oceans, zooplankton constitutes a key link in the food chain between primary producers and higher trophic levels. In the Arctic Ocean, they represent the most important prey of various higher trophic levels such as capelin and polar cod (Wassmann et al 2006). Changes in zooplankton communities could therefore have far-reaching consequences for the food web and commercial fishing.

Because of their low swimming ability and short life cycle (Wassmann et al. 2006) zooplankton respond easily to variability in the physical environment, such as temperature, algal biomass, and changes in oceanic current systems (Hays et al 2015). This makes them a good indicator of climate change in the marine environment and helps understand what role changes in the water mass circulations could play (Hays et al. 2005, Blachowiak 2008).

Warmer ocean temperatures and reduced sea ice coverage lead to a poleward shift of communities in the Arctic Ocean (Fossheim et al. 2015). This process has been termed “borealization” and is considerably changing Arctic marine food web structure with implications for ecosystem dynamics and functioning (Kortsch 2015).

Monitoring the community composition on a regular basis will help to better understand how the communities adapt to the changing environment and what the potential impacts, such as borealization, could mean for the arctic habitats.

The Arctic Ocean is the smallest ocean region, consisting of a deep basin surrounded by shelf seas with an average depth of 1050 meters (Pidwirny 2006), almost completely surrounded by land. The exchange with the Atlantic and Pacific oceans is limited. The shallow continental shelves surrounding the deep central basin have an average depth of 100 m (Jakobsson et al. 2003). These coastal areas are seasonal ice zones that receive 10% of the global river runoff and can sustain high productivity (Rudels et al. 1994, Schauer et al. 1997, Figure 1). The deep central basins on the other hand have been perennially ice-covered and are considered to be less productive (Sakshaug et al. 2004).

The central Arctic Ocean is subdivided into two basins by the Lomonosov Ridge: the Amerasian and Eurasian Basins (Jakobsson et al. 2003). The Eurasian Basin is subdivided in the Amundsen Basin and the Nansen Basin, separated by the Gakkel Ridge (Figure 1).

The dominant hydrographic feature of the Eurasian Basin is the Atlantic water (AW) inflow from the Nordic Seas. The Nansen Basin is affected by the Fram Strait inflow branch of the AW, as well as typical shelf water masses from the Barents Sea shelf. These two branches are interacting with each other and when meeting the two branches create intrusive layers, not only north of the Kara Sea between the main Barents Sea branch inflow but also north of Franz Josef Land, where a smaller fraction of the Barents Sea inflow enters the Nansen Basin (Rudels et al. 2013). Within the basin domain two basic water mass assemblies are observed, the difference between them being the absence or presence of Modified Atlantic Water (termed polar water by Bluhm et al. 2015) sandwiched between Polar Surface Water (termed Arctic Surface Water Bluhm et al. 2015) above and the AW below (Bluhm et al. 2015). The AW core is located rather shallow (100-200 m), however the whole Atlantic layer extends down to 750 m depth in the research area of this study (Nikolopoulos et al. 2018).

The Barents Sea is a shelf sea with depths ranging from 50 m at the shallow banks to 500 m at the deeper points (Sundfjord et al. 2007). The northern regions of the Barents Sea are seasonally covered by sea ice, with a maximum and minimum ice cover in April and September (Vinje and Kvambekk 1991). The Barents Sea is influenced by the confluence and mixing of different water masses. Warm, salty and nutrient-rich AW enters the Barents Sea from the southwest, overlain by Arctic Water that mixes with fresh meltwater (Sundfjord et al. 2007, Loeng 1991). The Barents Sea alone lost 50% of the annual ice cover between 1998 and 2009 (Årthun et al. 2012). Among other things, the vertical stratification of the waters has changed, which leads to a potentially higher penetration of vertical thermal convection into the warm, saline Atlantic layer. More heat and salt are consumed, leading to heating and salinification of the overlying Arctic water layer. In winter this leads to an additional loss of sea ice (Aksenov and Ivanov 2018).

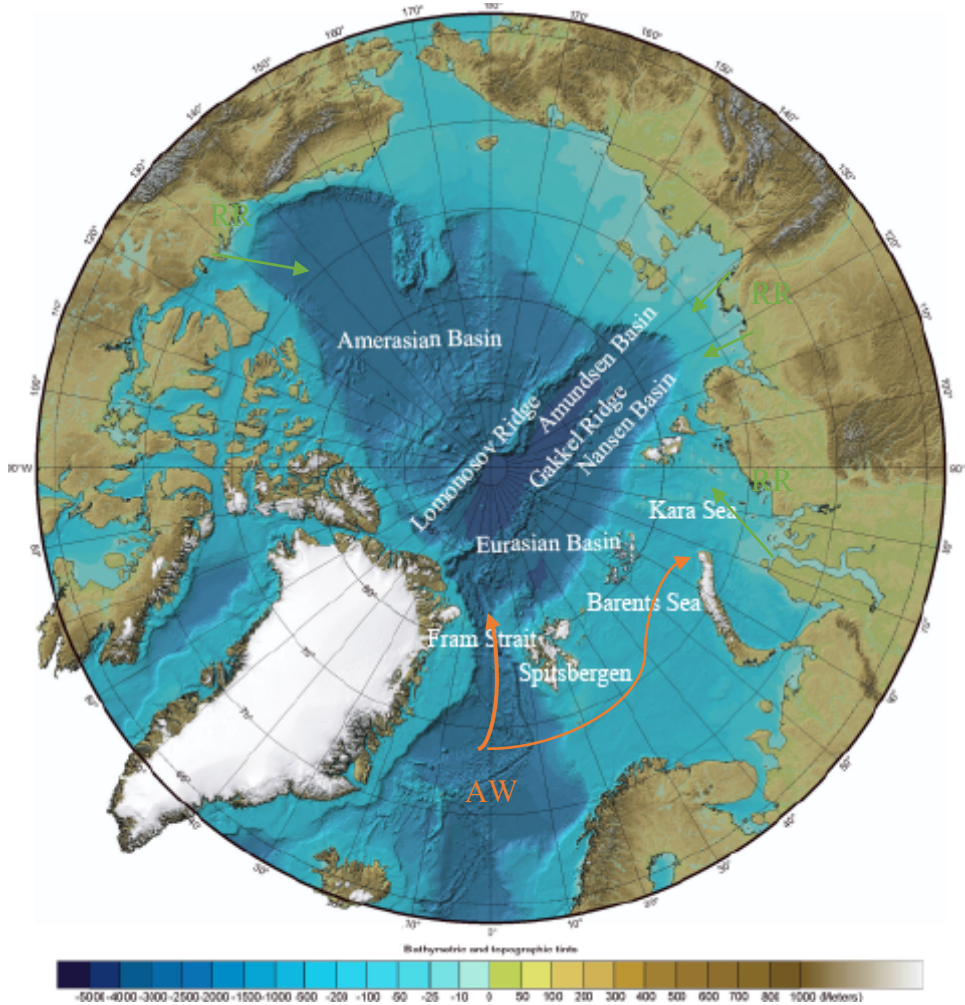


Figure 1: Bathymetric map of the Arctic Ocean, the orange arrows showing Atlantic water (AW) inflow and the green arrows the importance of riverine inflow (RR). Underlying map was obtained from NOAA, the National Oceanic and Atmospheric Administration (<https://www.ngdc.noaa.gov/mgg/bathymetry/arctic/currentmap.html>)

In terms of zooplankton biomass, the region is clearly dominated by Arctic copepods, predominantly *Calanus glacialis* Jaschnov, 1955, *Calanus finmarchicus* (Gunnerus 1770), *Calanus hyperboreus* Krøyer 1838 and *Metridia longa* (Lubbock 1854) (Falk-Petersen et al. 2009, Ksobokova 2009, David et al. 2015). *C. hyperboreus* and *C. glacialis* are considered Arctic endemic species and associated with cold Arctic water.

However, growing influence of AW in the Arctic could lead to a shift from the larger Arctic *Calanus* species toward the smaller Atlantic/boreal *C. finmarchicus*, therefore changing the community structure (Kortsch 2015). All the species have distinct life cycles, with *C. finmarchicus* having a one-year lifecycle in the Barents Sea, spawning in spring with the period of maximum phytoplankton bloom. *C. glacialis* often has a two-year lifecycle, and *C. hyperboreus* has the longest lifecycle lasting up to five or more years (Falk-Petersen et al. 2009).

Long time-series to monitor plankton and identify future changes in marine ecosystems are crucial (Hays et al. 2015). Traditional taxonomical analyses are not only time consuming, but greatly dependent on taxonomic expertise and hence expensive. This can lead to fragmented information that may be difficult to understand, because only a limited number of samples can be processed (Grosjean et al. 2004).

With new technology, such as the ZooScan, multiple organisms in a sample can be determined relatively quickly, and automatic prediction based on deep-learning algorithms saves time with identification (Benfield 2007). Unlike methods using DNA barcoding, the organisms do not have to be destroyed and can be kept for further investigations (Gorsky et al. 2010). Scanned organisms with attached metadata can also be shared between scientists for further analysis. Several scientists can work simultaneously on identifying organisms and correct previous identification if necessary. This could drastically reduce the number of identification mistakes. In addition, attached metadata can be used to carry out various calculations, such as determining abundances or biovolumes.

The goal of this bachelor thesis is to provide further information on the composition of epipelagic zooplankton communities in the Arctic Ocean determined by ZooScan image analysis (Grosjean et al. 2004) to verify whether there is a biogeographical and hydrographical pattern on the shelf and slope of the Barents Sea and in the Nansen Basin.

From the abundances determined with ZooScan, the corresponding biomass will be calculated and compared with the directly measured dry-weight biomass of the master thesis “Trophic structure and biomass of high Arctic zooplankton in the Eurasian Basin in 2017” by Nadezhda Zakharova (2019). Thereby it can be examined whether a taxonomic method such as ZooScan analysis leads to similar results as dry-weight measured biomass data. The study of zooplankton biomass by Zakharova (2019) showed unexpected results. The zooplankton biomass was highest on the shelf, but significantly lower on the slope than in the deep-sea-basin. Furthermore, no statistical differences in total biomass in relation of the influence of AW was confirmed, however smaller size fractions dominated stations more exposed to AW.

The detailed taxonomic results regarding abundances and biomasses, acquired by the ZooScan method, are examined further to investigate how biomass can act as proxy for abundance and community composition to further speed up sampling analyses.

The following **hypotheses** were therefore examined in the present study:

The variability of the zooplankton community mirrors biogeographical and hydrographical patterns along the Barents Sea shelf and into the Nansen Basin.

- A taxonomy-based optical method such as ZooScan analysis leads to similar results as dry-weight measured biomass data in terms of size distribution and total biomass.
- Biomass data can act as proxy for abundance in a taxonomically well-described ecosystem

2 Material and Methods

2.1 Sampling

The expedition PS 106/2 with the research vessel *Polarstern* provided an opportunity to sample the epipelagic zooplankton community from the shelf of the Barents Sea into the Nansen Basin proper, crossing a gradient of decreasing influence of Atlantic Water (AW).

From June 29, 2017, to July 13, 2017 the pelagic community was sampled with double-oblique hauls over a depth range of 0-100 m with a Rectangular Midwater Trawl (RMT). A detailed description of the sampling procedure during the cruise PS106.2 is available at Flores et al. (2018). Fifteen stations were sampled, of these, stations 52, 64, 65 and 83 were on the shelf and slope over a bottom depth of 135-553 meters. Stations 67 and 80 were located near the slope at a bottom depth of 2818 and 1849 meters, respectively. All remaining stations were taken in the Nansen Basin at a bottom depth of 2025-4022 meters (Figure 2, Table 1).

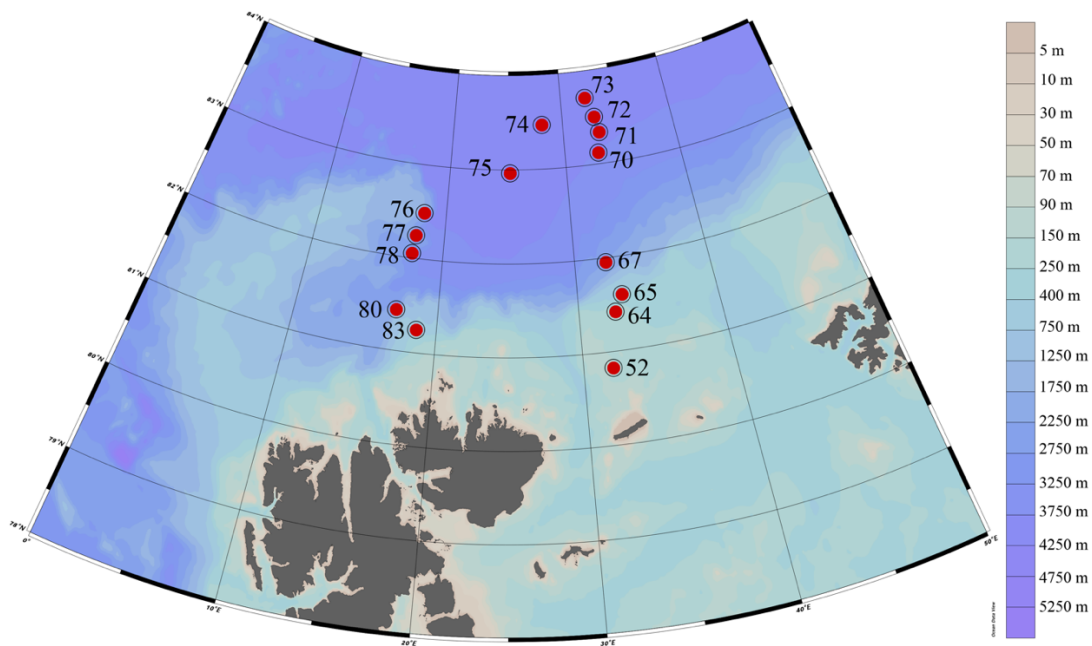


Figure 2: Overview of the RMT stations during the *Polarstern* expedition PS106.2

The RMT 1+8 has a pair of rectangular nets within the same frame, the RMT1 with a nominal mouth area of 1 m² and a mesh size of 320 μm and a larger RMT8 with a nominal mouth area of 8 m² and mesh size of 4.5 mm. The angle of these nets and hence their effective mouth areas, varies with the towing speed. At an angle of 45 degree the RMT1 has a mouth area of 1 m² and the RMT8 one of 8 m² (Roe et al. 1980). The mean towing speed of the research vessel was 2-3 knots. The volume of filtered water was estimated after Roe and Shale (1979).

For this study only the catch of the RMT-1 net was analyzed. On board, the samples were split in two halves with a Motoda plankton splitter (Motoda 1959). One half was preserved in 4% formaldehyde and transported to Alfred Wegener Institute (AWI) in Bremerhaven. The second half was fractionated in 6 size classes using a sieve tower, and each size fraction was frozen at -20°C for later dry mass analyses (Zakharova 2019). This study uses the formalin-preserved samples.

Table 1: Summary of RMT hauls conducted during PS106/2

Station	Date	Time [UTC]	Latitude	Longitude	Bottom depth (m)
52	29-06-2017	14:41	80.82638	31.953966	135
64	01-07-2017	14:48	81.41416	32.612201	204.4
65	02-07-2017	04:43	81.59516	33.207016	553
67	03-07-2017	12:18	81.95435	32.330701	2818.3
70	05-07-2017	20:58	83.11927	32.924238	3813.4
71	06-07-2017	05:32	83.334	33.237782	3902.6
72	06-07-2017	12:39	83.50125	32.981169	3982.7
73	07-07-2017	10:38	83.71395	32.337495	4022.3
74	08-07-2017	12:26	83.4679	28.085239	4049.1
75	09-07-2017	10:08	82.96345	25.135079	4045.9
76	10-07-2017	08:25	82.48965	18.224139	2277.8
77	10-07-2017	17:15	82.2445	17.782107	2024.9
78	11-07-2017	03:32	82.05043	17.643661	3155.8
80	12-07-2017	19:25	81.43483	17.034591	1849.4
83	13-07-2017	12:15	81.24548	18.605507	472.1

The study area is characterized by an inflow of AW from the Nordic seas and also by typical shelf water masses. Polar Surface Water (PSW) constituted the surface layer between the surface and about 50 to 150 m depth. Atlantic Water (AW) from below reached until a minimum depth of about 80 m. In-between these two water masses were the mixed products warm Polar Surface Water (wPSW) and Modified Atlantic Water (MAW) (Nikolopoulos et al. 2018). During the expedition PS 106/2 the AW reached up close to 100 m depth at the stations 52, 64, 65, 67, 70, 71, 78, 80 and 83 (Figure 2, 3). They were categorized as Atlantic-influenced stations. At the remaining stations 72, 73, 74, 75, 76 and 77, the AW stayed well below 400 m and the PSW layer reached as far down as about 150 m. These stations were categorized as polar-influenced stations.

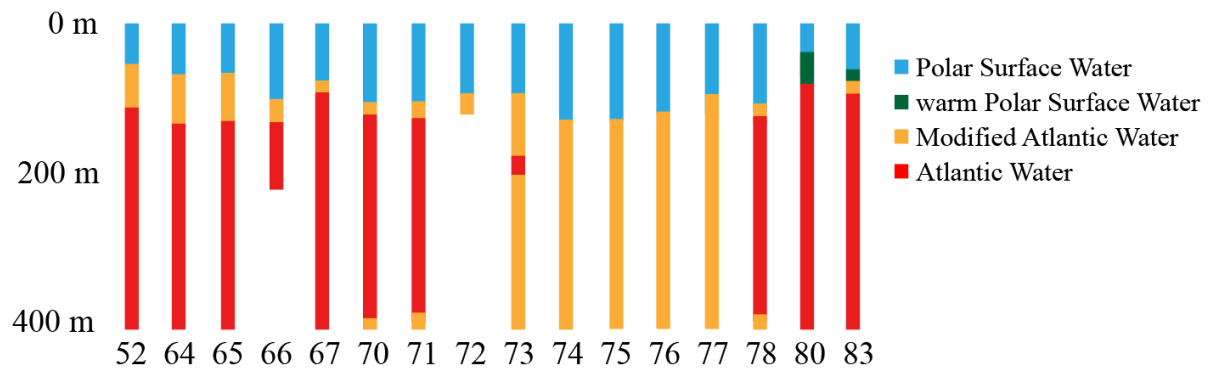


Figure 3: Water masses of upper 400 m at all station, hydrographic information by A. Nikolopoulos (unpublished data)

2.2 Sample analysis

After the samples were rinsed thoroughly with tap water to remove the formaldehyde, each sample was poured through a tower of sieves with decreasing mesh sizes (4000 μm , 2000 μm , 1000 μm , 500 μm , 250 μm , 125 μm , 64 μm) for size fractioning. The sieve tower was the same one that was used to separate the dry mass samples on board. This procedure allows an examination of the taxonomic composition separately within different size classes for later comparison with size-fractionated dry mass data.

The organisms of each subsample were transferred into a beaker prior to the scanning process. Subsamples with a high abundance of organisms were further split up into aliquots by a plankton splitter (Motoda 1959). The maximal split ratio was 1/256, no replicas were made.

To prevent superimposing animals on each other, it is recommended not to scan more than 1000-1500 organisms with the largest frame. However, this depends heavily on the body size of the organisms (Gorsky et al. 2010). To consider rare species it is recommended to use a sample size that is large enough to include at least a few individuals of every taxon (Grosjean et al. 2004). Therefore, the usage of varying mesh sizes which facilitates subsequent splitting, allowed for reducing the total amount of splits and the examination of larger sample sizes than otherwise possible (Vandromme et al. 2012).

2.3 ZooScan image analysis

We used a ZooScan (Model Biotom, Hydroptic, France) with a resolution of 2400 dpi (Gorsky et al. 2010). A transparent frame of the size of 15x24 cm was attached inside the waterproof flatbed scanner ZooScan. This frame determines the imaging area and allows processing the scan as a single image. The subsamples were then subsequently poured into the scanning cell. The frame has a 5 mm step and water is added above for avoiding the formation of a meniscus (Gorsky et al. 2010). Hereinafter all overlapping organisms were manually separated before the sample was scanned.

Lamps are integrated inside the top cover of the scanner to illuminate the chamber evenly. The cover also houses a reference cell for optical density. The transparent base of the scanner contains a high-resolution imaging device that permits scanning at a resolution of 2400 dpi. The base can be hinged which allows the recovery of the subsample without damage through a drainage channel after scanning (Gorsky et al. 2010). After scanning, all the samples were stored in 70% ethanol for further analysis or extended storage after the scanning process.

The images were then analyzed with the software application ZooProcess, a dedicated imaging software written in Java language for ImageJ and allowing automated processing and measurement of the scanned images. ZooProcess links the images with associated metadata and cuts the scanned image into multiple single images that ideally show no more than one organism (Gorsky et al. 2010). Images that still contain multiple or overlapping organisms were cut manually in the software and processed again.

The single images were uploaded into the web-based database EcoTaxa (Picheral et al. 2017), where they are automatically sorted by a two-way algorithm (random forest algorithm) and manually validated afterwards. An already existing Arctic learning set was used for the first automatic validation. This learning set included a collection of samples from the Fram Strait, containing almost all the taxa that would be expected in the samples of this study. The precision rate of automatic validation achieved an average of 60% (detailed information on all categories, recall and precision rate can be found in Figure A.1 A.2 and Table A.4), therefore a manual validation afterwards was necessary. Combined with the manual validation afterward, this semi-automatic process allows a more rapid classification of zooplankton compared to microscopy (Benfield 2007).

The organisms were classified to the lowest taxonomic level possible. Most copepods were determined up to genus level. In some cases, it was also possible to determine up to species level and different life stages (Table A.1/A.2). The 28046 classified images included 13558 non-biotic categories such as detritus, feces, artefact, fiber, and air bubbles. These categories were not considered in the analysis. Likewise, fallen antennas and legs, which made up 3470 images, were not included.

2.4 Abundance, Biovolume and Biomass

For further analysis, the image metadata acquired through EcoTaxa was exported into a tab-separated ASCII table.

To calculate the abundance, the option to export a summary with a count per category (taxon) and sample (i.e. size fraction) was chosen. It should be noted that each row of the table is a group (representing a taxon) of objects scanned by the ZooScan. A row contains the number of organisms scanned within the sample and annotated to this group. Each column of the table is one variable. The number of organisms per group and sample was then added up to represent the number of organisms for every group within one station.

Next, the abundance was calculated for every taxon of every station by multiplying the number of organisms with the on-board split ratio (as denominator, i.e. 2) and subsample ratio (as denominator, i.e. 64) from the lab. Next, it was divided by the water volume filtered during the haul.

$$Abundance = Abd \left[\frac{ind}{m^3} \right] = \frac{number\ of\ organisms * split-ratio * subsample\ ratio}{volume\ [m^3]} \quad (1)$$

A general export through EcoTaxa with the enabled options *Object Data*, *Process Data*, *Acquisition Data* and *Sample Data* was made for a calculation of biovolume. Each line of the table constitutes one object scanned by the ZooScan and each column of the table constitutes one variable.

An ellipsoid is considered the best representation of many organisms, including abundant copepods. Therefore, the elliptical model was chosen for the calculation of the biovolume, as it appears more realistic. Because the model is a function of both the projected size and the shape of each object and not only a function of the projected size (Vandromme et al. 2012). The primary axis for the best fitting ellipse of the object (major) and the secondary axis of the best fitting ellipse of the object (minor) were provided by EcoTaxa.

$$\text{Spherical Volume} = V (\text{mm}^3) = \frac{4}{3} * \Pi * \left[\frac{\text{Major (mm)}}{2} * \frac{\text{Minor (mm)}}{2} * \frac{\text{Minor (mm)}}{2} \right] \quad (2)$$

In the next step the spherical volume was multiplied with the subsample ratio (as denominator, i.e. 64) and split ratio (as denominator, i.e. 2) and then divided with the filtered water volume.

$$\text{Biovolume} = Bv \left(\frac{\text{mm}^3}{\text{m}^3} \right) = \frac{V * \text{split-ratio} * \text{subsample ratio}}{\text{volume} [\text{m}^3]} \quad (3)$$

Dry weight was calculated using the regressions between body area of an individual and its dry weight (Lehette and Hernandez-Leon 2009).

$$\text{Dry weight (DW)} = \frac{a * A^b}{1000} \quad (4)$$

The area (mm^2) of each individual was acquired by the image metadata through EcoTaxa and represented by A (the values of “*area excluded*” were used, in which the white areas within the object are excluded). *a* and *b* are the coefficients used following Table 2.

Table 2: Regression and correlation parameters obtained from Lehette and Hernandez-Leon (2009)

Organism	a	b	r	P	Source Organism	Source
Calanus finm./glac.	56.43	1.44	0.777	<0.001	Calanus propinquus	Hernandez-Leon and Montero 2006
Calanus hyperboreus	76.71	0.63	0.518	<0.001	Rhincalanus gigas	Hernandez-Leon and Montero 2006
Metridia longa	22.44	1.78	0.797	<0.001	Metridia gerlachei	Hernandez-Leon and Montero 2006
Euphausiacea	87.45	1.34	0.967	<0.001	Euphausia superba	Hernandez-Leon and Montero 2006
Crustacea	43.97	1.52	0.972	<0.001	General crustaceans	Hernandez-Leon and Montero 2006, Lehette and Hernandez-Leon, 2009
Cnidaria, Clione limacina	4.03	1.24	0.902	<0.001	Salps sp.	Lehette and Hernandez-Leon, 2009
Chaetognatha	23.45	1.19	0.840	<0.001	Chaetognatha	Lehette and Hernandez-Leon, 2009
All other groups	43.38	1.54	0.947	<0.001	General mesozooplankton	Hernandez-Leon and Montero 2006, Lehette and Hernandez-Leon, 2009

Due to high variability in the taxonomy, many groups did not fit the regression line of the coefficients of general mesozooplankton, therefore various coefficients for different groups were used. The coefficients of *salps sp.* were used as most representative for gelatinous organisms like Cnidaria and *Clione limacina* based on the findings of Giering et al. (2019).

Biomass density was then calculated by multiplying the DW with the split-ratio (as denominator, i.e. 2) and subsample ratio (as denominator, i.e. 64) and then dividing with the filtered water volume

$$Biomass\ density = Bm \left(\frac{mg}{m^3} \right) = \frac{DW * split-ratio * subsample\ ratio}{volume [m^3]} \quad (5)$$

The biomass of each taxon at one station was estimated as the sum of the individual biomasses from every organism.

2.5 Statistical analysis

The Mann-Whitney-U test, also called Wilcoxon rank sum test (Wilcoxon 1945) was used to test the significance of differences between the median value of two groups for different parameters (Table A.3). This is a non-parametric test that compares two unpaired groups, more precisely the distribution of ranks in two groups. H₀ states that the two groups are part of one population, the rank distributions of values in both groups are identical. The p-value describes the probability that H₀ is confirmed. The level of significance α constitutes the p-value below which the probability that the two groups belong to a single population is considered so low that a “significant difference” is assumed, and the null hypothesis (H₀) is rejected. For the purpose of this study, α was set to 0.05, following a widely used convention.

Statistical analysis was carried out using the IBM SPSS Statistics software.

The Shannon-Wiener species diversity index (Shannon and Weaver 1949) is defined as

$$H' = - \sum (p_i * \log(p_i)) \quad (6)$$

with n_i being the number of individuals of a species i and $p_i = \frac{n_i}{N}$ representing the share of a species compared to the total individual number (N) in a sample.

Pielou's evenness (Pielou 1969) is defined as

$$J' = \frac{H'}{H'_{max}} \quad (7)$$

Where H' is the number derived from the Shannon-Wiener diversity and H'_{max} is the maximum possible value of H' , equal to $H'_{max} = \ln(S)$. With S being the total number of species.

In order to reveal similarities and dissimilarities in the community structure between stations in the study area, a cluster analysis was performed. The abundances of all taxa found at the stations were analyzed. The cluster analysis was performed with R version 1.2.5019 (R Core Team 2020) using the *vegan* (Oksanen et al. 2013) and *graphics* (R Core Team 2020) packages. The abundance data was log transformed and a hierarchical clustering of the zooplankton abundance and species composition was carried out for Bray-Curtis-Similarity matrixes (Bray-Curtis 1957), a complete linkage method was used.

3 Results

3.1 Description of the taxa, community composition and taxa abundance

The mesozooplankton community from the shelf of the Barents Sea to the Nansen Basin proper was clearly dominated by copepods. *Calanus finmarchicus/glacialis* and *Calanus hyperboreus* were the dominant copepod species. The non-copepod community was mainly composed of Chaetognatha, Appendicularia, Amphipoda, Euphausiacea, Cnidaria, Isopoda and Ostracoda. The highest abundance was recorded at station 80 (216 ind. m⁻³) in the Sophia Basin. This was followed by station 52 on the shelf (94 ind. m⁻³). The lowest abundance was found at station 76 (13 ind. m⁻³) in the Nansen Basin. Overall, the stations with the lowest abundance were all found in the Nansen Basin (Table 3, Figure 1).

The cluster analysis, based on Bray-Curtis dissimilarity, revealed two different clusters (Figure 4). Cluster 1 contains all stations strongly influenced by AW within 20 m of the depth range sampled in this study. Cluster 2 is separated from the other cluster at a dissimilarity of 0.7 and consists of stations where the AW was well below the sampling depth of the RMT, because layers of Polar Surface Water and Modified Atlantic water overlaid the AW (Figure 2). Only Station 71 was grouped together with these stations although at this station the AW did almost reach the sampling depth of the RMT (Figure 2). Henceforth, Cluster 2 will be referred to as the polar regime (PR) and Cluster 1 as Atlantic regime (AR).

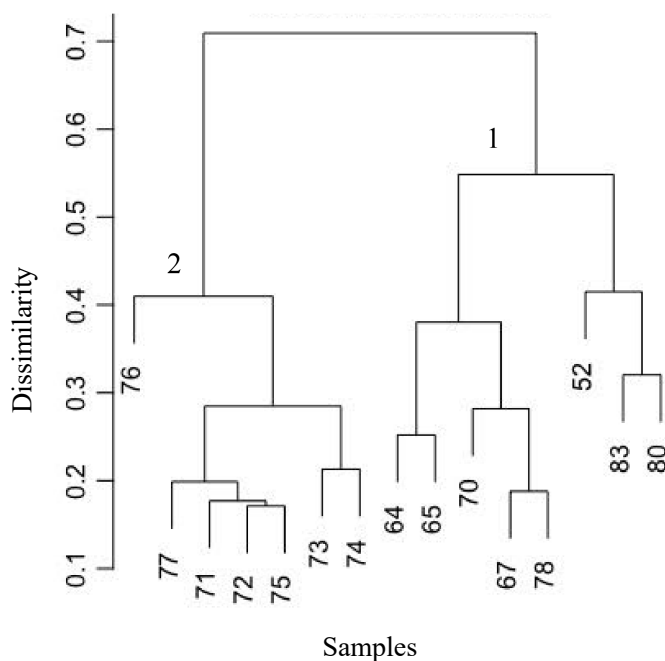


Figure 4: Results of cluster analysis of 15 stations (samples), analysis based on Bray Curtis similarity. With cluster numbers 1 and 2.

The AR contains all stations situated on the shelf or influenced by the shelf slope. Only Stations 70 and 78 were situated in the deeper Nansen Basin. Stations of the AR had significantly higher overall abundances than the stations of the PR (Mann-Whitney U test; $W = 30$, $p = 0.001$, Table A.3).

Concerning the abundance of mesozooplankton in the study area, both a spatial and a size-dependent pattern were observed.

At most stations, the relative abundance was dominated by the 1000-2000 μm size-fraction (average 49.7%). Only at station 65, 80 and 83 on the shelf slope, relative abundances in the 500-1000 μm size-fraction (45%, 50%, 45% respectively) were slightly higher than the 1000-2000 μm size-fraction (44%, 38%, 40% respectively).

At stations 52 and 70 the total abundance of size-fraction 1000-2000 μm was 3 to 4 times higher than the next highest size-fraction. At station 52 and 80 the total abundance of the 250-500 μm size-fraction was noticeably above-average (Table 3, Figure 5).

Table 3: Total number of taxa and combined abundance of all taxa at the sampling sites. Split in size-fractions.

Station	Total taxa number	Total abundance (ind. m^{-3})	64-250 μm	250-500 μm	500-1000 μm	1000-2000 μm	2000-4000 μm	>4000 μm	Cluster
52	27	94.09	0.17	20.21	18.90	51.82	2.74	0.26	AR
64	23	35.39	0.22	2.10	10.74	21.57	0.49	0.27	AR
65	20	27.10	0.36	1.94	12.19	11.89	0.63	0.09	AR
67	18	42.06	0.19	4.35	16.28	20.74	0.50	0.00	AR
70	17	67.53	0.12	1.22	13.05	50.59	2.45	0.10	AR
71	19	29.21	0.32	2.87	8.45	14.84	2.59	0.14	PR
72	16	23.77	0.31	2.85	5.28	11.29	3.57	0.47	PR
73	17	15.12	0.15	1.89	3.47	7.67	1.22	0.72	PR
74	17	22.93	0.23	3.11	6.70	10.40	1.99	0.50	PR
75	19	31.71	0.46	3.47	6.86	15.92	4.22	0.78	PR
76	17	12.97	0.22	2.19	1.96	5.96	2.03	0.61	PR
77	18	25.28	0.11	1.68	9.15	9.96	3.08	1.30	PR
78	18	61.80	0.34	2.93	16.72	38.84	2.43	0.54	AR
80	18	216.10	0.65	21.36	96.39	85.97	10.68	1.04	AR
83	21	59.44	0.18	6.04	29.71	22.57	0.59	0.35	AR

Table 4: Abundance of all Copepods at the sampling sites. Split in size-fractions.

Station	Total abundance Copepods (ind. m ⁻³)	64-250 µm	250-500 µm	500-1000 µm	1000-2000 µm	2000-4000 µm	>4000 µm	Cluster
52	90.77	0.15	19.81	18.15	50.00	2.57	0.09	AR
64	33.85	0.18	1.75	10.31	21.22	0.35	0.04	AR
65	23.83	0.30	1.37	10.04	11.53	0.54	0.05	AR
67	38.69	0.16	3.79	14.40	19.90	0.44	0.00	AR
70	58.92	0.09	0.67	8.85	47.19	2.10	0.02	AR
71	24.27	0.29	2.19	6.11	13.82	1.84	0.02	PR
72	19.33	0.26	1.81	3.52	10.36	3.26	0.12	PR
73	11.76	0.12	1.34	2.07	6.76	1.14	0.33	PR
74	17.25	0.18	2.25	2.76	9.93	1.89	0.24	PR
75	26.67	0.30	2.80	3.63	15.61	3.94	0.39	PR
76	9.18	0.17	1.24	0.56	4.97	1.90	0.34	PR
77	18.22	0.07	0.68	5.23	9.21	2.52	0.51	PR
78	54.33	0.24	2.00	15.03	34.83	2.04	0.19	AR
80	202.47	0.49	19.28	92.74	80.24	9.51	0.21	AR
83	55.8	0.17	4.99	28.55	21.63	0.33	0.13	AR

Table 5: Abundance of all taxa within different size-fractions, both Clusters and overall in ind. m⁻³, median, 25%, 75% quantile (Q.) and average with standard deviation.

Size-fraction (µm)	64-250	250-500	500-1000	1000-2000	2000-4000	>4000	PR	AR	Abundance overall
Median (ind. m ⁻³)	0.22	2.87	10.74	15.90	2.43	0.47	23.80	60.60	31.71
25% Q. (ind. m ⁻³)	0.18	2.00	6.80	10.90	0.90	0.20	19.03	40.40	24.52
75% Q. (ind. m ⁻³)	0.33	3.91	16.50	30.71	2.91	0.66	27.25	74.17	60.62
Average ± standard deviation (ind. m ⁻³)	0.27 ±0.14	5.2 ±6.4	17.1 ±23	25.3 ±22.3	2.6 ±2.5	0.48 ±0.4	23 ±6.9	75.4 ±60.6	50.97 ±50.88

In total the mesozooplankton community of the study area consisted of 34 taxa, 17 of which were classified as copepod species and 17 were non-copepod taxa. 26.5% of all taxa appeared at all stations. More than half of all taxa (56%) appeared at 8 or more stations. The highest number of taxa appeared at Station 52 (27 taxa), followed by the other stations situated on the shelf or influenced by the shelf slope (20-23 taxa). Stations 71 and 75 had the highest number in the Nansen Basin with 19 taxa. The lowest number of taxa was at station 72 with 16 taxa. (Table A.1/A.2). The number of taxa of stations in the AR (average 19.4) was significantly higher than the number of taxa of stations in the PR (average 16.4) (Mann-Whitney U test; $W = 37$, $p = 0.029$, Table A.3).

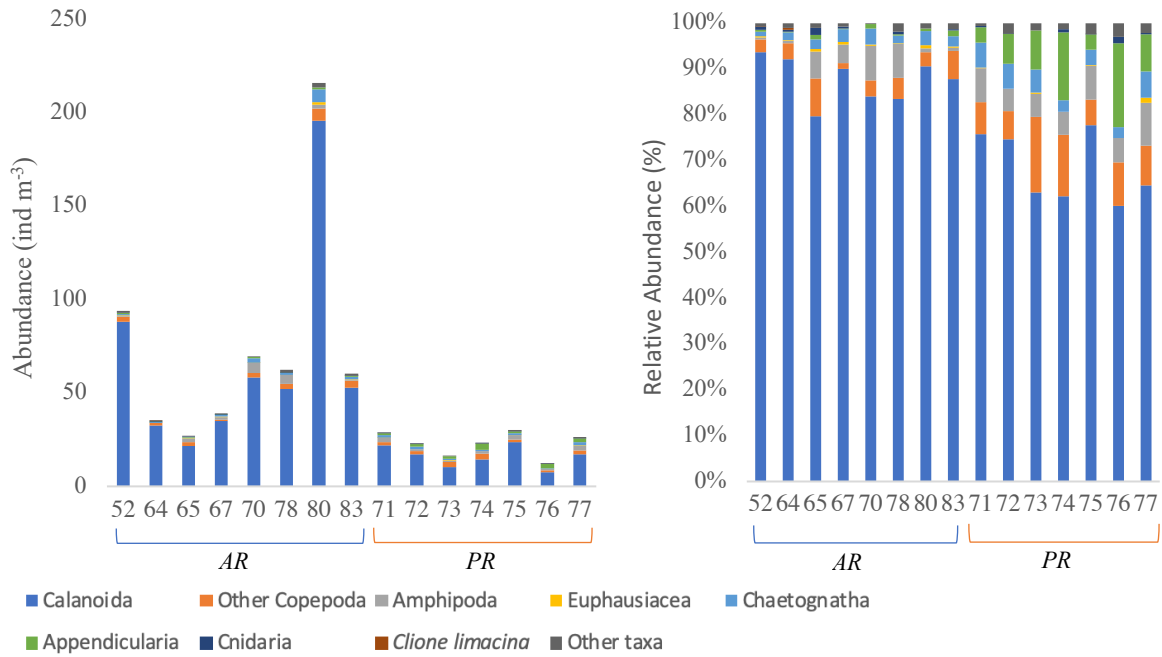


Figure 5: Taxonomic composition at all stations. Abundances (left panel) and relative abundances (right panel). Copepoda with a contribution < 4% are grouped as “Other Copepoda” and non-copepod taxa with contribution <1% are grouped as “Other Taxa.”

The diversity index of Shannon Wiener (H) and evenness were calculated for all stations (Table 6). The highest H was found at station 74 (2.10) and station 73 (2.09), respectively as well as the highest evenness with 0.59 at both stations. The lowest H was found at station 64 (0.74), as well as the lowest evenness with 0.21. The H and evenness values of the PR stations were significantly higher than values of the AR stations. (Mann-Whitney U test; $W = 36$, $p < 0.001$, Table A.3).

Table 6: Shannon-Wiener Index and Evenness of all stations

Station	H	Evenness
52	1.12	0.32
64	0.74	0.21
65	1.36	0.39
67	1.65	0.47
70	1.41	0.40
78	1.44	0.41
80	1.27	0.36
83	0.99	0.28
71	1.85	0.52
72	1.98	0.56
73	2.09	0.59
74	2.10	0.59
75	1.93	0.55
76	2.05	0.58
77	2.00	0.57

3.2 Copepods

Copepods dominated the mesozooplankton community at all stations and accounted for 89.65% of the overall abundance in the study area. The distribution varied slightly across the investigation area.

The copepod community consisted of 17 identified taxa, from 12 different families, as well as unidentified Copepoda, Calanoida and nauplii that could not be determined to species level.

However, these unidentified taxa only contributed 2.5% of the total copepod community.

Male copepods accounted for less than 0.05% to the mesozooplankton community and were therefore combined with the females of their respective taxon.

Table 7: Abundance of copepods at all stations, median, quartile (Q.) and average (Avr.) with standard deviation (SD) of all taxa in ind. m⁻³,

Station	Calanus finm./glac.	Calanus hyperboreus	Metridia longa	Other Calanoida	Other Copepoda	Nauplii
52	64.07	3.25	1.91	18.97	1.48	0.22
64	27.62	0.66	2.61	1.73	0.78	0.16
65	18.59	1.25	0.06	1.70	0.94	0.07
67	23.12	2.37	5.58	3.96	2.61	0.00
70	39.78	8.29	8.26	2.07	0.12	0.00
78	37.17	2.56	10.26	2.09	1.51	0.08
80	139.88	3.13	37.06	15.89	4.23	1.24
83	47.15	1.11	1.88	2.85	2.13	0.70
71	13.52	3.44	3.17	1.68	1.84	0.00
72	8.05	6.00	2.02	1.23	1.29	0.21
73	4.57	2.18	2.66	0.94	0.83	0.06
74	5.45	4.35	3.74	1.01	2.15	0.17
75	9.15	5.54	8.24	0.61	2.40	0.20
76	1.22	2.34	3.75	0.19	1.24	0.18
77	10.31	3.31	2.24	1.18	0.40	0.22
Median	18.59	3.13	3.17	1.70	1.48	0.17
25% Q.	8.60	2.26	2.13	1.10	0.88	0.07
75% Q.	38.47	3.89	6.91	2.47	2.14	0.21
Avr.±SD	29.98±35.37	3.32±2.03	6.23±8.99	3.74±5.66	1.60±1.03	0.23±0.33

Table 8: Total relative abundance of copepods at each station in %

Station	Calanus finm./glac.	Calanus hyperboreus	Metridia longa	Other Calanoida	Other Copepoda	Unidentified nauplii
52	71.27	3.61	2.12	21.10	1.65	0.24
64	82.29	1.95	7.78	5.15	2.33	0.49
65	82.20	5.53	0.26	7.53	4.14	0.33
67	60.30	6.18	14.56	10.32	6.82	1.81
70	67.97	14.17	14.12	3.53	0.21	0.00
78	69.35	4.78	19.14	3.90	2.82	0.00
80	69.87	1.56	18.51	7.94	2.11	0.00
83	85.23	2.00	3.39	5.15	3.85	0.37
71	56.98	14.51	13.38	7.10	7.77	0.26
72	42.91	31.96	10.77	6.57	6.90	0.89
73	40.16	19.14	23.43	8.23	7.30	1.73
74	32.39	25.75	22.19	5.98	12.73	1.07
75	35.00	21.17	31.49	2.34	9.17	0.83
76	13.88	26.59	42.51	2.13	14.01	0.87
77	55.19	17.70	12.00	6.33	2.17	6.62
Average	57.66	13.11	15.71	6.89	5.60	1.03

The highest abundance of copepods was found at station 80 (202.47 ind. m⁻³), followed by station 52 (90.76 ind. m⁻³). The lowest abundance of copepods appeared at station 73 (11.77 ind. m⁻³) and 76 (9.18 ind. m⁻³) (Table 7). Overall, the stations with the lowest abundance of copepods were all found at stations in the PR (Mann-Whitney U test; $W = 30$, $p = 0.001$, Table A.3).

Calanus finmarchicus/glacialis, *Calanus hyperboreus* and *Metridia longa* dominated at all stations, compared to other Calanoida and other Copepoda. The AR was characterized by a dominance of *Calanus finmarchicus/glacialis*, while the PR was characterized by *Metridia longa* and *Calanus hyperboreus*. The relative abundance of *C. finm./glac.* in the PR was lower than in the AR (Mann-Whitney U test; $W = 26$, $p < 0.001$, Table A.3), and vice versa for *C. hyperboreus* (Mann-Whitney U test; $W = 36$, $p < 0.001$, Table A.3).

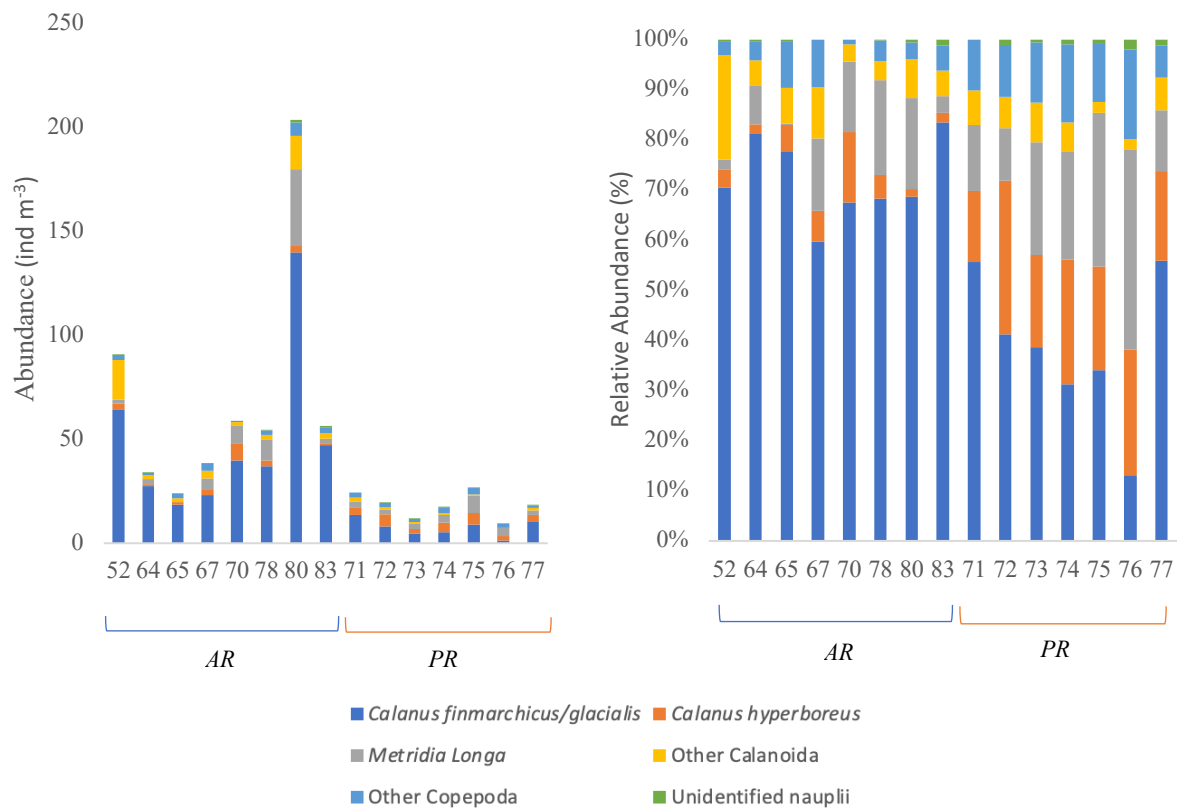


Figure 6: Species composition of copepods at all stations. Abundances (left panel) and relative abundances (right panel). Copepods with contribution <4% were grouped as “Other Copepoda”, Calanoida with contribution <3% were grouped as “Other Calanoida”.

3.3 Selected copepod taxa

Hereafter, the abundance and stage composition of the dominant taxa *C.*

finmarchicus/glacialis, *C. hyperboreus* and *Metridia longa* are examined in more detail in order to analyze spatial patterns within their stage composition.

3.3.1 *Calanus finmarchicus/glacialis*

Calanus finmarchicus/glacialis played a major role in the total copepod community with regard to abundance (Table 8). Similar as for all copepods highest abundances were found at station 80 (139.88 ind. m⁻³) and 52 (64.07 ind. m⁻³) and lowest at station 76 (1.22 ind. m⁻³).

Overall the adult stages, together with the older copepodite stages (copepodite stage CIV) and CV) dominated at most stations, especially in the Nansen Basin. Copepodite stage CIII was abundant at station 80 and 83, while almost being absent at all other stations.

In general, copepodite stages CI-CIII showed spatial patterns and were mostly found close to or on the shelf and slope. The highest abundance of stage CII was found at station 80 and 83 (17.41 ind. m⁻³, 5.93 ind. m⁻³, respectively) while the highest abundance of stage CI was found at station 52 (13.71 ind. m⁻³), but CI were also abundant at station 80 and 83 (6.64 ind. m⁻³, 2.31 ind. m⁻³, respectively). Generally, *C. finmarchicus/glacialis* showed a pattern when comparing the two clusters, by having higher contributions in the AR.

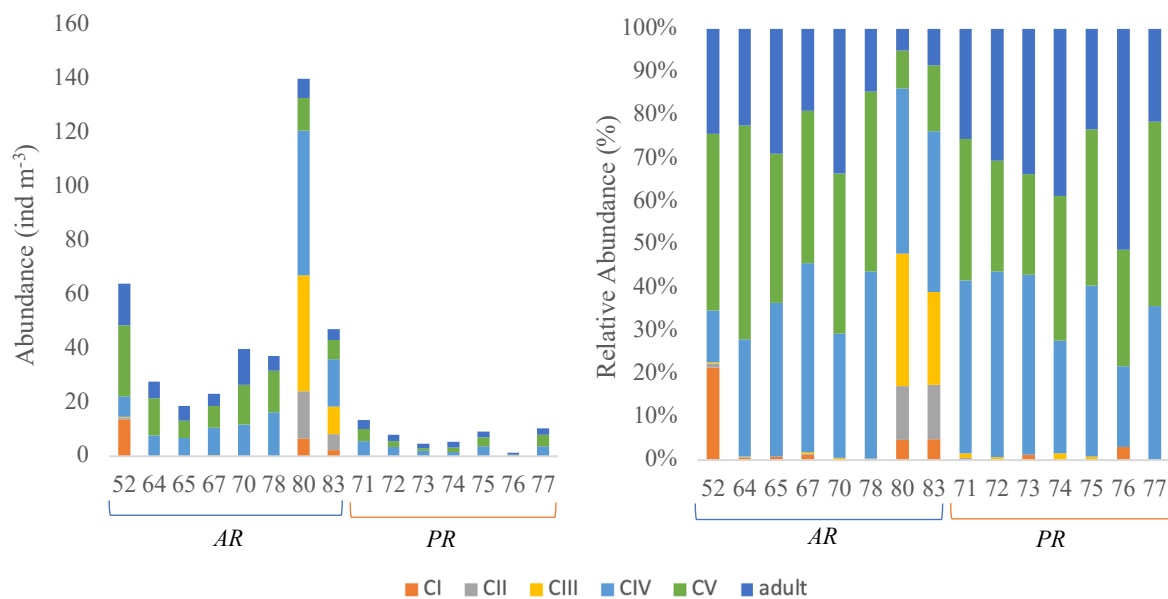


Figure 7: Developmental stage composition of *Calanus finmarchicus/glacialis* at all stations. Abundances (left panel) and relative abundances (right panel).

3.3.2 *Calanus hyperboreus*

The adult stages had low contributions ranging from 0.02% to 1.35% on the AR stations and high contributions on the PR stations, with the highest contribution at station 76 with 16.31%. (Table 8). Stage CV had especially high abundances at station 52 and 70 (2.45 ind. m⁻³, 4.36 ind. m⁻³, respectively), while stage CIII had the highest abundance at station 80 (1.04 ind. m⁻³), followed by station 70 (0.7 ind. m⁻³), showing generally higher abundance on the AR stations.

When comparing the two clusters, *Calanus hyperboreus* had a major contribution at stations in the PR and therefore showed a different spatial pattern compared to the other *Calanus* species (Table 7).

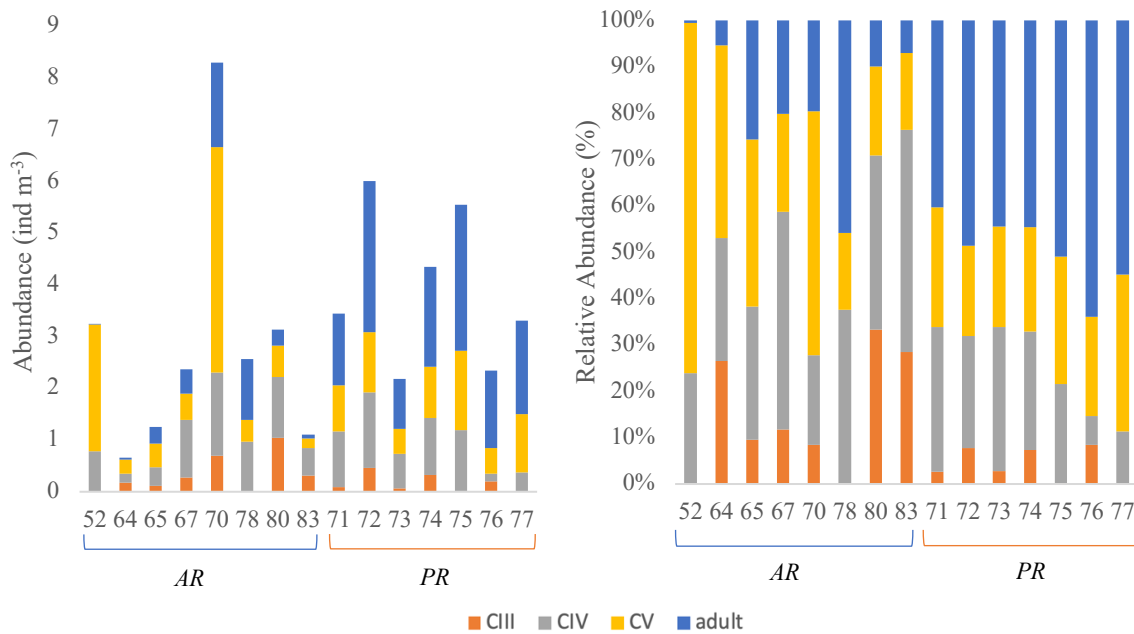


Figure 8: Stage composition of *Calanus hyperboreus* at all stations. Abundances (left panel) and relative abundances (right panel).

3.3.3 *Metridia longa*

Only the adult stage and CV stage were identified in *Metridia longa*, with the adult stage being dominant at all stations (except for station 65). *Metridia longa* showed spatial patterns by having low abundances on the shelf and slope (Table 7). The highest abundance was found at station 80 (37.06 ind. m⁻³) and the lowest abundance at station 65 (0.06 ind. m⁻³). The adult stage was absent at station 65, while the CV stage was absent at station 75.

The stage composition of *Metridia longa* showed no pattern when the two clusters were compared.

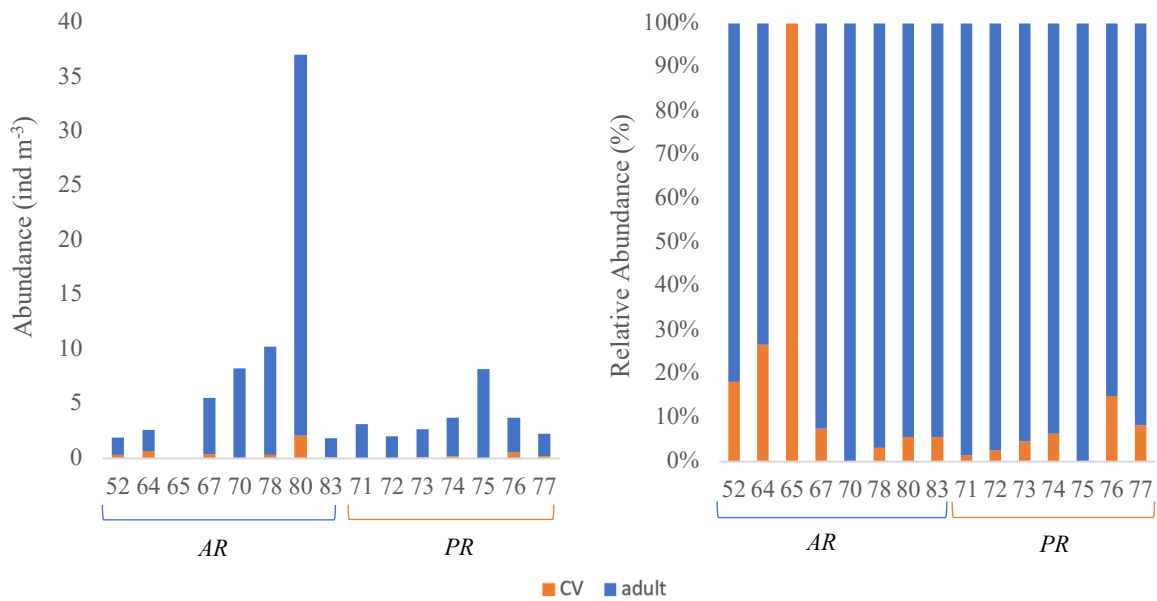


Figure 9: Stage composition of *Metridia longa* at all stations. Abundances (left panel) and contribution (right panel).

3.4 Non-copepod taxa

Non-copepod taxa accounted for 10.3% of the total abundances of the mesozooplankton community in the study area.

The highest abundance of non-copepods was found at station 80 (13.63 ind. m⁻³), followed by station 70 (8.68 ind. m⁻³). The lowest abundance of non-copepods appeared at station 64 (1.54 ind. m⁻³). All stations with lowest abundance of non-copepods were found at AR stations. However, the abundance of non-copepods at all AR stations was not significantly lower than at PR stations (Mann-Whitney U test; $W = 58$, $p = 0.536$, Table A.3).

For a consideration of the species composition the non-copepod taxa with an occurrence of less than 1% within the non-copepod community were summarized as “other taxa”.

Chaetognatha, Appendicularia and Amphipoda occurred at all stations (Figure 10). Fish larvae and *Bivalvia* were only found at station 52.

In addition, Siphonophorae, *Clione limacina*, Polychaeta, Trochophora larvae and fish larvae were only found on the shelf and slope, with low abundances less than 0.1 ind. m⁻³, except for a higher abundance of 0.14 ind. m⁻³ of *Clione limacina* at station 64.

None of the non-copepod taxa was clearly dominant over all stations (Figure 10, Table 9). However, Chaetognatha were well distributed throughout the study area, with the highest abundance at station 80 (6.6 ind. m⁻³). Chaetognatha had a higher contribution at AR stations, compared to PR stations, however not significantly (Mann-Whitney U test; $W = 52$, $p = 0.694$, Table A.3). Appendicularia were significantly stronger represented at PR stations compared to AR stations (Mann-Whitney U test; $W = 38$, $p = 0.001$, Table A.3), with the highest abundance at station 74 (3.47 ind. m⁻³).

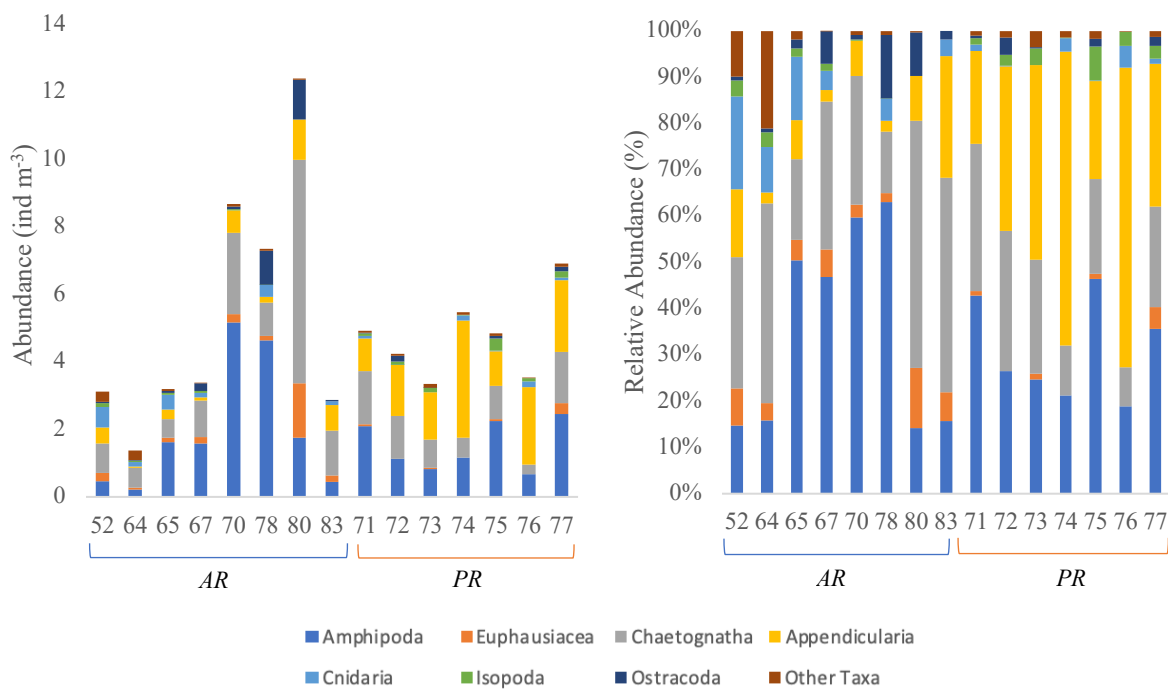


Figure 10: Species composition of non-copepods at all stations. Abundances (left panel) and relative abundance (right panel). Taxa with contribution <0.05% were grouped as “Other Taxa”

Table 9: Abundance of non-copepods at all stations, median, quartile (Q.) and average (Avr.) with standard deviation (SD) of all taxa in ind. m⁻³,

Station	Amphipoda	Euphausiacea	Chaetognatha	Appendicularia	Cnidaria	Isopoda	Ostracoda	Other taxa
52	0.46	0.25	0.88	0.46	0.62	0.11	0.03	0.31
64	0.22	0.05	0.60	0.03	0.14	0.04	0.01	0.29
65	1.61	0.14	0.56	0.27	0.44	0.06	0.06	0.06
67	1.58	0.20	1.07	0.09	0.14	0.05	0.23	0.00
70	5.18	0.25	2.41	0.66	0.00	0.02	0.09	0.07
78	4.63	0.14	0.98	0.17	0.35	0.01	1.00	0.07
80	1.76	1.61	6.61	1.20	0.00	0.00	1.17	0.03
83	0.45	0.18	1.34	0.75	0.10	0.00	0.05	0.00
71	2.10	0.05	1.56	0.98	0.07	0.07	0.02	0.05
72	1.12	0.00	1.28	1.51	0.00	0.10	0.16	0.06
73	0.83	0.04	0.83	1.41	0.00	0.12	0.01	0.12
74	1.16	0.00	0.59	3.47	0.16	0.01	0.00	0.08
75	2.25	0.05	1.00	1.02	0.01	0.35	0.08	0.08
76	0.67	0.00	0.30	2.29	0.17	0.11	0.00	0.01
77	2.46	0.33	1.50	2.13	0.07	0.20	0.13	0.09
Median	1.58	0.14	1.00	0.98	0.10	0.06	0.06	0.07
25% Q.	0.75	0.04	0.71	0.37	0.01	0.02	0.02	0.04
75% Q.	2.18	0.22	1.42	1.46	0.16	0.11	0.14	0.08
Avr.±SD	1.77±1.45	0.22±0.40	1.43±1.52	1.10±0.96	0.15±0.18	0.08±0.09	0.20±0.37	0.09±0.09

3.5 Biovolume and Biomass

The biovolume was calculated from all fifteen stations of the RMT1 (Figure 11) and was then converted into biomass in terms of dry mass.

After converting biovolume into biomass, the contribution of size-fractions shifted, especially towards the 1000-2000 µm size-fraction (Table 10). This size-fraction accounted for about half of the total biovolume but had a contribution of 67% to the total biomass. The size-fraction 500-1000 µm also doubled its contribution to the total biomass compared to the contribution it had to the total biovolume. The contribution of the 2000-4000 µm and >4000 µm size-fraction halved in the contribution to the total biomass compared to the contribution to the total biovolume.

Within the stations, the contribution also shifted slightly after the conversion. Stations 52 and 80, in particular, had a higher contribution to the total biomass compared to the contribution to the total biovolume (Table 11).

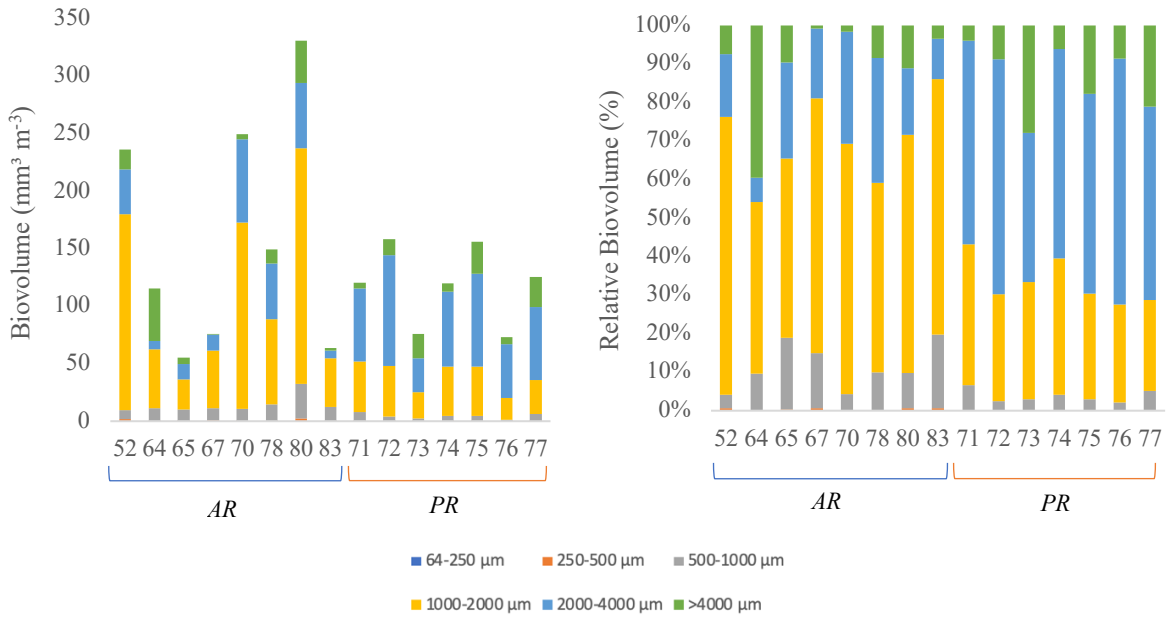


Figure 11: Biovolume in $\text{mm}^3 \text{m}^{-3}$ at all stations (left panel) and biovolume contribution at all stations (right panel). Split in size-fractions.

However, there was a significant positive relationship between the calculated biovolume, based on the data acquired through ZooScan and the converted biomass (Figure 12).

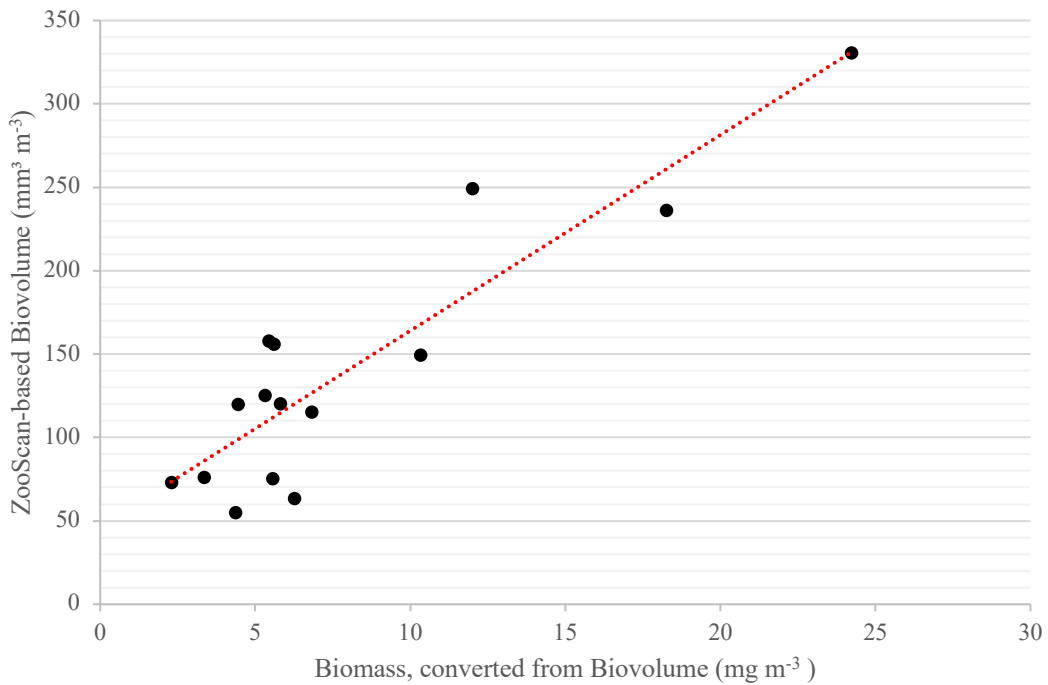


Figure 12: Relationship between ZooScan-based biovolume and biomass converted from the biovolume, with linear trend-line. There is a significant positive relationship. Linear regression: $y = 11.74x + 46.574$ $R^2 = 0.81$, $p < 0.001$

Table 10: Contribution of size-fractions for zooplankton biomass and biovolume in %

Size-fraction	64-250 μm	250-500 μm	500-1000 μm	1000-2000 μm	2000-4000 μm	>4000 μm
Biomass in %	0.01	0.54	12.44	67.05	14.48	5.49
Biovolume in %	0.01	0.31	6.55	48.71	33.42	11.01

Table 11: Contribution over all stations for zooplankton biomass and biovolume in %

Station	Biomass (%)	Biovolume (%)
52	15.21	11.23
65	5.67	5.48
65	3.63	2.62
67	4.63	3.59
70	10.01	11.85
78	8.60	7.10
80	20.19	15.71
83	5.21	3.03
71	4.84	5.71
72	4.52	7.51
73	2.79	3.62
74	3.70	5.70
75	4.66	7.41
76	1.91	3.48
77	4.42	5.96

The highest biomass was recorded at station 80 (24.2 mg m^{-3}), located close to the slope. Followed by station 52 (18.2 mg m^{-3}), located on the shelf. A high biomass was also found at station 70 (11.9 mg m^{-3}), located high north in the Nansen Basin. The lowest biomass was found at station 76 (2.3 mg m^{-3}) in the western part of the Nansen Basin (Figure 14). There was a significant difference between the median biomass for the AR (8.6 mg m^{-3}) and the PR (5.3 mg m^{-3}), (Mann-Whitney U test; $W = 35$, $p = 0.014$, Figure 13, Table A.3).

At all stations, the 1000-2000 μm size-fraction had the highest contribution (62.6% on average), while the 64-250 μm size-fraction had the lowest contribution (0.0011% on average). The size-fraction 1000-2000 μm was most dominant at station 52 (84%) and station 70 (80.2%). At the station with one of the lowest biomasses, station 73, there was a higher contribution of the >4000 μm size-fraction (20%), higher than at all other stations (6.9% on average). The size-fraction 64-125 μm did not occur at this station. There was also a high contribution of the >4000 μm size-fraction at station 77 (14.5%) (Figure 14)

At the PR stations, there was a higher contribution of size-fraction 2000-4000 μm (21.6% on average), compared to the AR stations (6.2% on average).

The contribution of the size-fractions 1000-2000 μm (70.4%) and 500-1000 μm (17.3%) was somewhat higher on AR stations than on PR stations. (59.7% and 10.9%, respectively).

Stations grouped as the PR had overall lower biomass and a pronounced contribution of the larger size fractions >4000 μm and especially 2000-4000 μm compared to the AR. In addition, the 500-1000 μm size-fraction was less pronounced at stations of the PR than in the AR (Figure 14).

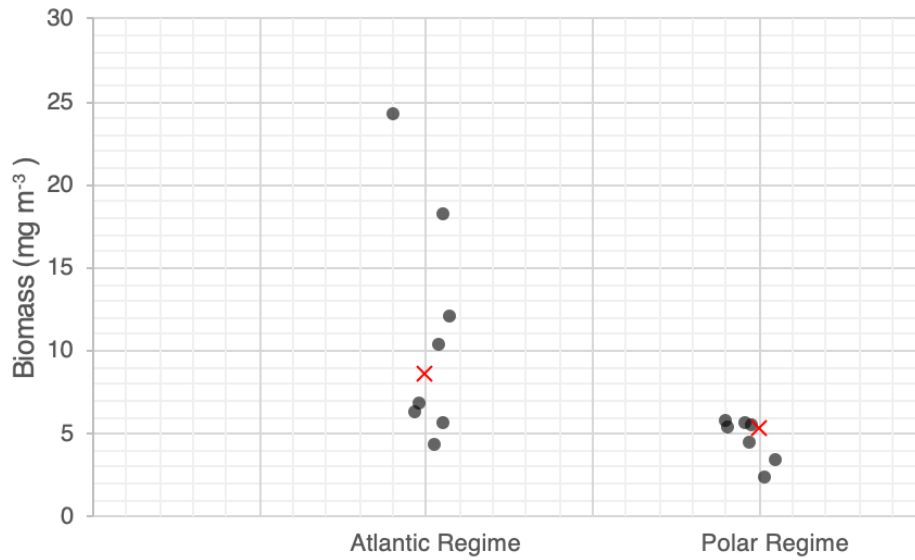


Figure 13: Total biomass (mg m^{-3}) of all 15 stations, split by cluster. Median values marked as red crosses (x).

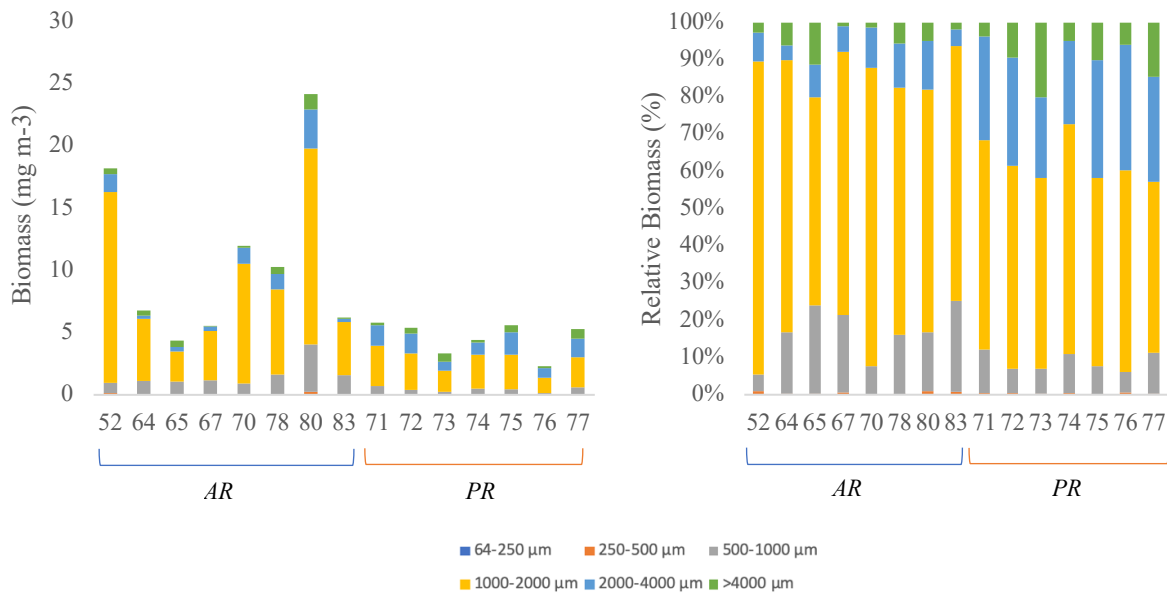


Figure 14: Biomass in mg m^{-3} at all stations (left panel) and biomass contribution at all stations (right panel). Split in size-fractions.

3.6 Composition of size-fractions

The taxonomic composition for the size-fractions showed the highest contribution of Copepoda in the size-fraction 1000-2000 μm (92.21%), the size-fraction that also made up the largest contribution to the total biomass. Copepod's contribution to the size-fraction 500-1000 μm (87.43%) was similarly high. The size-fraction $> 4000 \mu\text{m}$ mainly had a high contribution of Chaetognatha (41.73%), but also the highest contribution of Euphausiacea (14.94%). In the smaller size-fractions, Chaetognatha and Euphausiacea did not have a high contribution. With smaller size-fractions, the contribution of Appendicularia increased. In size-fraction 250-500 μm 26.47% and in size-fraction 64-250 μm 29.96%. The size-fraction 64-250 μm also had the largest contribution of Amphipoda (18.16%) (Figure 15, Table 13). Copepoda had the highest biomass in all size-fractions, except for size-fraction $>4000 \mu\text{m}$, where Chaetognatha had the highest biomass (3.28 mg m^{-3}). Euphausiacea also had a higher biomass than copepods in size-fraction $>4000 \mu\text{m}$. Amphipoda had the highest biomass in size-fractions 1000-2000 μm (0.91 mg m^{-3}) and about half as high biomass in size-fraction 500-1000 μm , 2000-4000 μm , and $>4000 \mu\text{m}$. The highest biomass of Euphausiacea was found in the size-fraction of 2000-4000 μm (1.7 mg m^{-3}) Appendicularia had the highest biomass in size-fraction 1000-2000 μm (1.15 mg m^{-3}) and Cnidaria in size-fraction 500-1000 μm (0.05 mg m^{-3}) (Figure 15, Table 12).

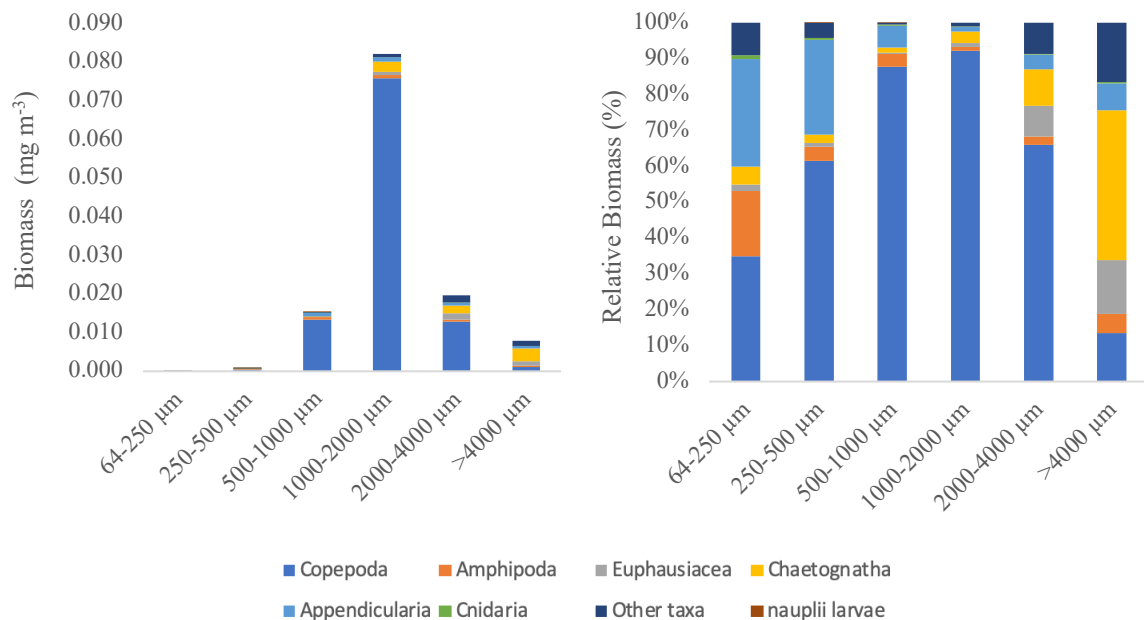


Figure 15: Total biomass in mg m^{-3} for all size-fractions (left panel) and biomass contribution for all size-fractions in % (right panel).

Table 12: Total biomass of taxa, median, quartile (Q.) and average (Avr.) with standard deviation (SD) of all taxa in mg m⁻³, split in size-fractions.

Size-fraction	64-250 µm	250-500 µm	500-1000 µm	1000-2000 µm	2000-4000 µm	>4000 µm
Copepoda	0.007	0.495	13.424	75.668	12.902	1.070
Amphipoda	0.004	0.031	0.571	0.907	0.461	0.417
Euphausiacea	0.000	0.008	0.038	0.802	1.699	1.176
Chaetognatha	0.001	0.019	0.209	2.616	1.959	3.286
Appendicularia	0.006	0.213	0.934	1.145	0.814	0.591
Cnidaria	0.000	0.005	0.050	0.048	0.045	0.030
Other taxa	0.002	0.033	0.082	0.871	1.699	1.303
nauplii	0.000	0.000	0.005	0.000	0.000	0.000
Total	0.020	0.805	15.314	82.057	19.580	7.874
Median	0.001	0.025	0.146	0.889	1.256	0.831
25% Q.	0.000	0.007	0.047	0.614	0.357	0.320
75% Q.	0.004	0.078	0.662	1.513	1.764	1.208
Avr.±SD	0.003±0.003	0.101±0.174	1.914±4.662	10.257±26.442	2.447±4.294	0.984±1.056

Table 13: Total biomass contribution of taxa in %, split in size-fractions.

Size-fraction	64-250 µm	250-500 µm	500-1000 µm	1000-2000 µm	2000-4000 µm	>4000 µm
Copepoda	35.01	61.52	87.66	92.21	65.90	13.59
Amphipoda	18.16	3.89	3.73	1.10	2.36	5.30
Euphausiacea	1.81	1.01	0.25	0.98	8.68	14.94
Chaetognatha	4.92	2.38	1.36	3.19	10.00	41.73
Appendicularia	29.96	26.47	6.10	1.40	4.16	7.51
Cnidaria	1.18	0.59	0.33	0.06	0.23	0.39
Other taxa	8.97	4.12	0.54	1.06	8.68	16.55
nauplii	0.00	0.03	0.04	0.00	0.00	0.00

Calanus hyperboreus had the highest contribution in size-fraction 2000-4000 µm (61.8%) and >4000 µm (56.3%). Likewise, *Metridia longa* had a high contribution especially in the size-fraction 1000-2000 µm (21%), 2000-4000 µm (11.6%) and >4000 µm (9.2%). *Calanus finmarchicus/glacialis* had the highest contribution in size-fraction 500-1000 µm (94.29) and were also very present in other size-fractions. However, the proportion of *Calanus finmarchicus/glacialis* was very small in size-fraction >4000 µm (6.19%).

In the 64-500 µm size-fraction, less common Calanoida and Copepoda were found, which were classified as "Other". Likewise, unidentified nauplii (mainly from Copepoda) were found mainly in the size-fraction 64-250 µm (Figure 16, Table 15).

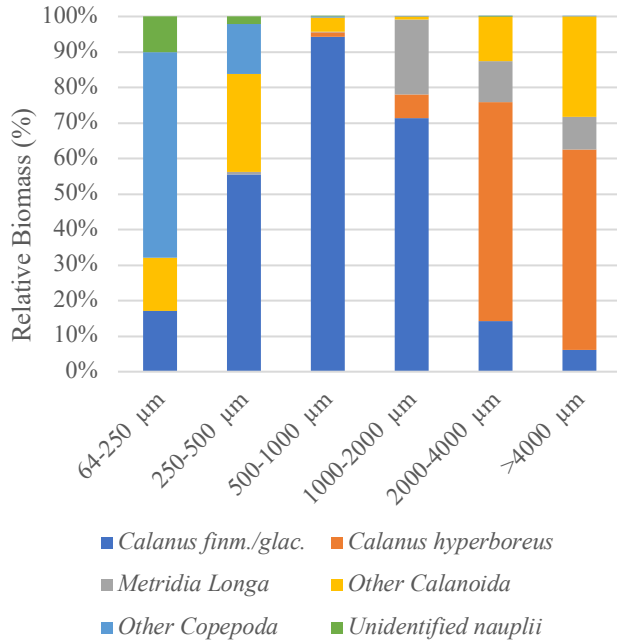


Figure 16: Total biomass contribution (%) of Copepoda taxa, split in size-fractions

Table 14: Total biomass of Copepoda ($mg\ m^{-3}$), split in size-fractions.

Size-fraction	64-250 µm	250-500 µm	500-1000 µm	1000-2000 µm	2000-4000 µm	>4000 µm
Calanus finm./glac.	0.001	0.281	12.658	53.980	1.826	0.066
Calanus hyperboreus	0.000	0.00	0.162	5.099	7.968	0.603
Metridia longa	0.000	0.003	0.037	15.881	1.491	0.099
Other Calanoida	0.001	0.139	0.532	0.704	1.616	0.302
Other Copepoda	0.005	0.071	0.035	0.003	0.001	0.000
Unidentified nauplii	0.001	0.010	0.000	0.000	0.000	0.000
Total	0.008	0.505	13.424	75.668	12.903	1.070
Median	0.001	0.041	0.100	2.902	1.553	0.082
25% Q.	0.000	0.005	0.036	0.178	0.374	0.017
75% Q.	0.001	0.122	0.439	13.186	1.774	0.251
Avr.	0.001	0.084	2.237	12.611	2.150	0.178
±SD	±0.002	±0.111	±5.109	±21.158	±2.964	±0.236

Table 15: Total biomass contribution of Copepods (%), split in size-fractions.

Size-fraction	64-250 µm	250-500 µm	500-1000 µm	1000-2000 µm	2000-4000 µm	>4000 µm	Avr.
Calanus finm./glac.	17.06	55.61	94.29	71.34	14.15	6.19	43.11
Calanus hyperboreus	0.00	0.00	1.20	6.74	61.76	56.30	21.00
Metridia longa	0.15	0.65	0.28	20.99	11.56	9.22	7.14
Other Calanoida	14.94	27.57	3.96	0.93	12.52	28.25	14.70
Other Copepoda	57.90	14.12	0.26	0.00	0.01	0.04	12.06
Unidentified nauplii	9.96	2.05	0.00	0.00	0.00	0.00	2.00

3.7 Comparison of Abundance, Biovolume and Biomass

There was a significant positive relationship between biomass and abundance (Figure 17).

There was also a significant positive relationship between biovolume and abundance (Figure 18). However, values differed more widely between biovolume and abundance.

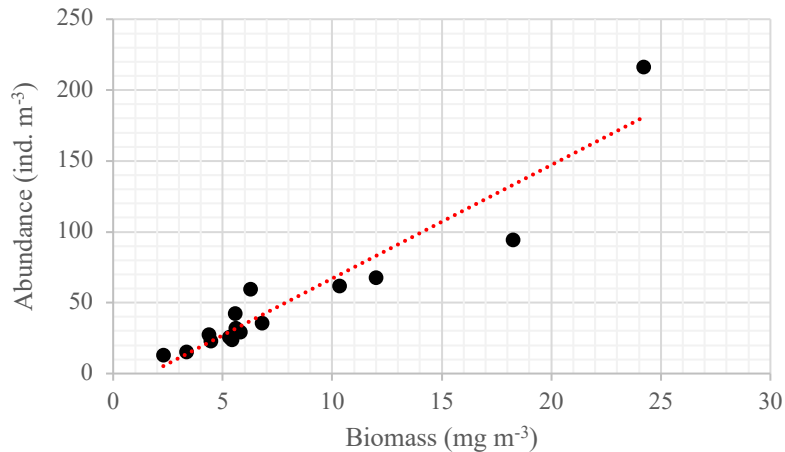


Figure 17: Relationship between biomass and abundance, with linear trend-line. There is a significant positive relationship. Linear regression: $y = 8.0109x - 13.072$ $R^2 = 0.89$, $p < 0.001$)

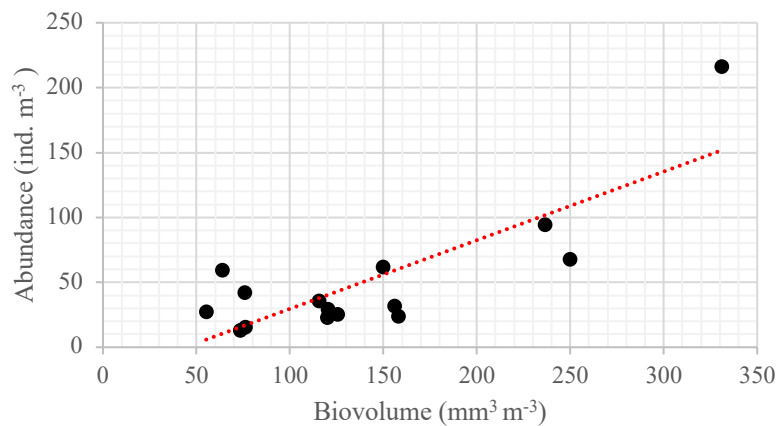


Figure 18: Relationship between biovolume and abundance, with linear trend-line. There is a significant positive relationship. Linear regression: $y = 0.5288x - 23.282$ $R^2 = 0.66$, ($p < 0.001$)

In order to examine the relationship within the size-fractions between the abundance and the biomass, the most dominant group Copepoda was examined in more detail. The biggest differences were found in the smallest and largest size-fractions. Copepoda contributed to just under half of the biomass in the 64-250 μm size-fraction, while they accounted for 70% of abundance in this size-fraction. In the $> 4000 \mu\text{m}$ size-fraction, their contribution to the biomass was also smaller than their contribution to the abundance (Table 16).

Within all other size-fractions, there was a similar relationship between biomass and abundance.

Table 16: Total relative contribution of biomass and abundance in %, split in size-fractions.

Size-fraction	64-250 μm	250-500 μm	500-1000 μm	1000-2000 μm	2000-4000 μm	>4000 μm
Biomass (%)	49.8	77.7	90.6	94.1	74.3	16.3
Abundance (%)	69.5	83.1	86.5	93.9	87.1	37.3

3.8 Comparison of ZooScan-based biomass and dry weight biomass

The results of the ZooScan-based biomass were compared with the biomass directly measured from dry weight (Zakharova 2019). Stations 75, 80 and 83 were not considered, because they were contaminated with sand and particles of the ship and therefore it was impossible to estimate the dry weight biomass of these stations in Zakharova (2019). Twelve stations in total were compared. There was a positive relationship between both methods ($p=0.004$, $R^2 = 0.573$) (Figure 19). However, certain deviations could be recognized. The biomass determined with ZooScan was on average almost twice as high as the measured dry weight biomass (Table 17). The dry weight measured biomass was highest at station 78, while the ZooScan-based biomass was highest at station 52. In general, the ZooScan-based method showed higher biomasses on the shelf and slope, while the dry weight measured biomass showed higher values in the Nansen Basin, apart from station 52 (Table 17).

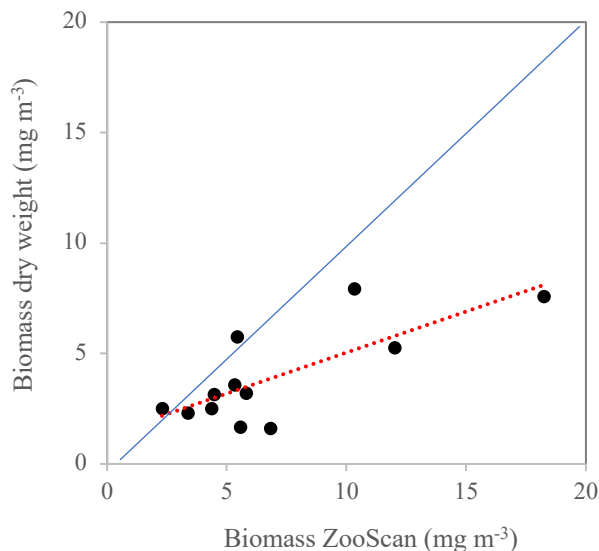


Figure 19: Relationship between ZooScan-based biomass and dry weight measured biomass, with linear trend-line. Blue line indicates 1:1 relationship. There is a significant positive relationship. Linear regression: $y = 0.3714x + 1.3301$ ($R^2 = 0.573$, $p = 0.004$)

Table 17: Comparison of biomass values between biomass measured by dry weight and ZooScan-based biomass, median, quartile (Q.) and average (Avr.) with standard deviation (SD) in mg m⁻³.

Station	Biomass dry weight (mg m ⁻³)	Biomass ZooScan (mg m ⁻³)
52	7.60	18.24
64	1.60	6.80
65	2.53	4.35
67	1.67	5.56
70	5.27	11.99
71	3.20	5.80
72	5.75	5.42
73	2.31	3.34
74	3.16	4.44
76	2.50	2.29
77	3.60	5.30
78	7.94	10.32
Total	47.11	83.86
Median	3.18	5.49
25% Q.	2.45	4.42
75% Q.	5.39	7.68
Avr.±SD	3.93±2.20	6.99±4.48

Based on my data, the size-fraction distribution of station 52 measured by dry weight is not comprehensible, because the 1000-2000 µm size-fraction was entirely missing, while the 500-1000 µm size-fraction takes up most of the station. Therefore station 52 was omitted for the following comparison. However, stations 52 was still considered for previous comparison.

The ZooScan-based biomass showed the highest contribution of the 1000-2000 µm size-fraction, while the 2000-4000 µm and >4000 µm size-fraction had a slightly higher contribution for the dry weight measured biomass and distribution of size-fraction 1000-2000 µm was lower compared to ZooScan-based biomass (Figure 20).

Biomass for the 64-250 µm and 250-500 µm size-fraction was low determined with both methods.

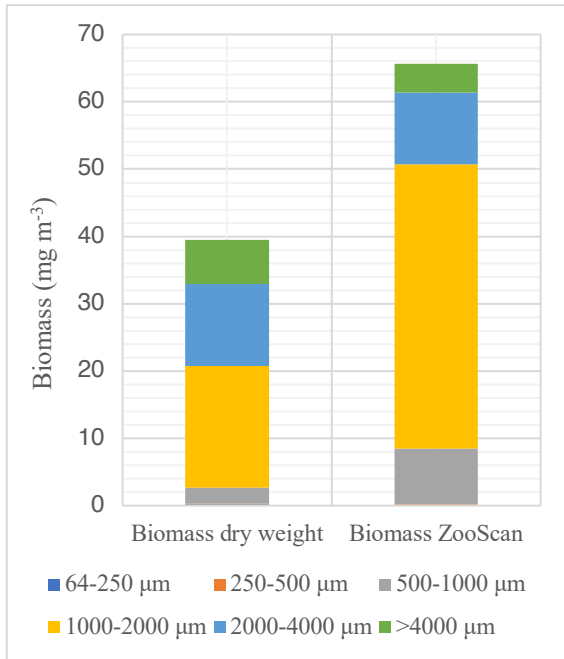


Figure 20: Accumulated biomass of all stations, split in size-fractions

The 2000-4000 μm size fraction showed a positive relationship between both methods ($R^2 = 0.710$, $p = 0.001$), without heavily over- or underestimating one of the methods. However, the 1000-2000 μm ($R^2 = 0.420$, $p = 0.031$) and especially 500-1000 μm ($R^2 = 0.582$, $p = 0.006$) size-fractions showed a tendency to overestimate the ZooScan-based biomass (Figure 21).

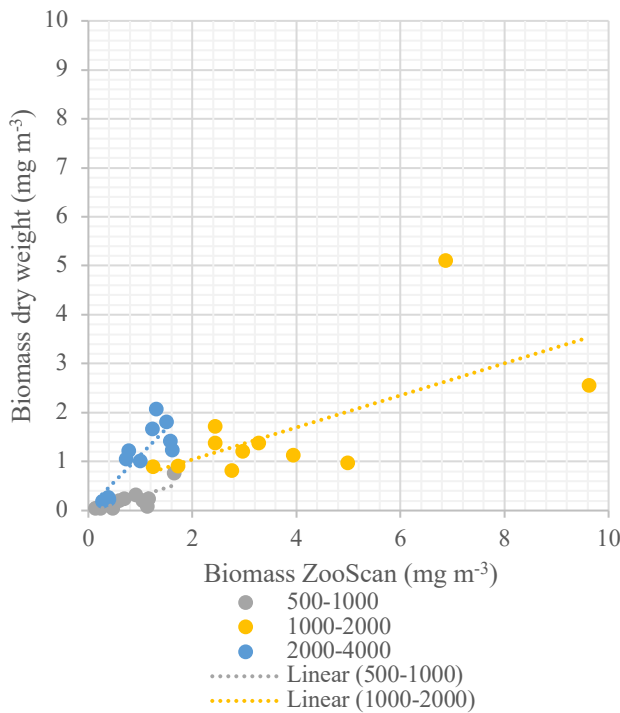


Figure 21: Exemplary relationship between ZooScan-based biomass and dry weight measured biomass with trendline, for the size-fractions 500-1000 μm (gray), 1000-2000 μm (yellow) and 2000-4000 μm (blue).

4 Discussion

For a better understanding of the changing Arctic environment and potential impacts, such as borealization, monitoring of the zooplankton community composition on a regular basis is crucial. With the present bachelor thesis changes in the community composition, abundance and biomass of epipelagic zooplankton were analyzed from the shelf of the Barents Sea to the Nansen Basin, crossing a gradient of decreasing influence of Atlantic Water (AW).

Present results and previously reported findings show that the mesozooplankton community from the shelf of the Barents Sea to the Nansen Basin proper was clearly dominated by copepods (Daase 2007, Kosobokova 2009, Thibault 1998). Notably, *C. finmarchicus/glacialis* and *C. hyperboreus* were the dominant copepods, as expected and shown in previous studies (Thibault 1998, Kosobokova 2009, David et al. 2015). There are not many reports of early spring abundances in the study area for comparison, moreover differences in the analysis between microscopic studies and the ZooScan method limit the comparability with other studies. In this thesis, the abundance ranged from 12.5 ind. m⁻³ to 216 ind. m⁻³ with an average of 51 ind. m⁻³ and median of 30.3 ind. m⁻³. Previously reported studies show similar results with an average of 50.6 ind. m⁻³ and median of 43 ind. m⁻³ (Thibault 1998).

Results showing higher abundances than this study were sampled when plankton blooms appeared, since the Eurasian Arctic regions are affected by seasonal patterns (Kosobokova 1982). For instance, a phytoplankton bloom has been recorded at station 80 (Castellani et al. 2019), where the highest abundance was found. A global increase in water temperature is expected to change the phytoplankton community structure. Consequently, this is leading to a cascading effect of food web dynamics and the structure of the marine food web (Finkel et al. 2009). This is important, because abundances correspond well with *Chlorophyll a* concentration, supporting the reproduction of copepods, since the ingested phytoplankton carbon fuels the reproduction energy (Thibault 1998, Matsuno 2012).

A spatial trend was observed in the Atlantic regime (AR), showing high abundance values on the shelf and slope and gradually decreasing abundance towards the basins. Likewise, lowest values were recorded by previous studies in the Nansen Basin (Thibault 1998) which were sampled in summer. However, different patterns could be found within the stations located in the Nansen Basin. This regional variability is most likely related to the circulation patterns, as highest biomass was found in the core of the Atlantic inflow. The basin domain is characterized by two basic water masses. The Atlantic regime (AR) with near-surface Atlantic Water (AW) and the polar regime (PR) with AW at a greater depth, overlain with polar surface water and intermediate water (Bluhm et al. 2015, Nikolopoulos et al. 2018). Accordingly, two main clusters of the community structure were found in this study that corresponded to these regimes. Only station 71 was grouped with the PR, even though the CTD profile was typical for the AR. This station was located in the border region between Atlantic- and polar-influenced surface waters. The CTD and RMT stations can be a few miles apart, therefore the station probably showed the fauna of the PR, while the CTD still measured AW influences near the surface.

Large organisms (>2000 μm) were mainly represented in the PR of the Nansen Basin. However *Calanus* species such as *C. finmarchicus* and *C. glacialis* were less dominant in the deeper polar regime of the Nansen Basin. A growing influence of AW in the Arctic Ocean might change the community structure, leading to a shift from the larger Arctic species *C. glacialis* and *C. hyperboreus* toward the smaller boreal *C. finmarchicus* (Kortsch 2015). This study can neither confirm nor deny the shift, because the species *C. finmarchicus* and *C. glacialis* were merged in the taxon *Calanus finmarchicus/glacialis*. On the other hand, species typical for the high-arctic such as *C. hyperboreus* were mainly found in the PR of the Nansen Basin.

The distribution patterns show that mainly adult animals were found in the deeper areas of the Nansen Basin, however earlier stages may have been underrepresented in all the samples due to the coarse mesh size of the RMT-1. It is also possible that reproduction was delayed in the deeper Nansen Basin compared to the shelf and slope regions (Matsuno 2012). This interpretation is in agreement with low numbers of nauplii larvae caught with the Multinet in deep waters, compared to the shelf (N. Hildebrandt, personal communication). Overall, only a few males were found, which are mainly found between late autumn and late spring, seldom in summer (Daase 2018).

The taxonomic composition comprised at least 34 taxa. Identification with ZooScan probably led to a somewhat biased representation of taxonomic diversity. Important taxonomic information is lost due to the inevitable merging of species and categories, as confirmed by earlier studies (Bell and Hopcroft 2008, Gislason and Silva 2009, Gorsky et al. 2010). This leads to lower species numbers than, for example, microscopic analysis. Only organisms laying on the scanner cell bottom will be in focus and transferring samples creates air bubbles, causing organisms to float on top.

Additionally, smaller organisms are generally difficult to identify (Rolke and Lenz 1984, Wickline 2016). Organisms with some of the smallest size examined in this study were mainly *Oithona* spp. and small copepods, other small organisms included younger stages of larger species, which therefore were probably underrepresented in this study. In this study 69% of all copepods labeled as "bad focus" were in the 64-500 μm size-fraction showing that smaller species are more likely to be out of focus. Considering that the "bad focus" category only amounted to 1.6% of the total community, this source of error is negligible, however small rare species might be underrepresented. Therefore, coloring small species could lead to improved identification due to higher contrast (Rolke and Lenz 1984). Nevertheless, species cannot be examined from several angles and precisely measured, even less than in a microscopic analysis. As a result, there may always be difficulties in identifying all organisms precisely.

The polar regime in the Nansen Basin also showed the highest diversity, because they were not primarily dominated with high numbers of *C. finmarchius* and *C. glacialis*, leading to the assumption that an increase of AW in Arctic waters could lead to a decline in biodiversity, despite an increase in total abundance. In accordance with previous reported studies (19 to 42 mg m^{-3} (Thibault 1998), 3.3 to 14.3 mg m^{-3} (Hirche 2011), 1.9 to 23.9 g m^{-2} (Kosobokova 2009)), the biomass ranged from 2.29 to 24.2 mg m^{-3} (0.3 to 2.42 g m^{-2}). Differences, however, will always occur due to the high spatial, seasonal and inter-annual variability of zooplankton abundance. Furthermore, methodical aberrations depending on the used sampling methods and mesh sizes limit the comparability of different studies (Kosobokova 2009). The RMT1 has a mesh size of 320 μm , which means that smaller species in particular, may be underrepresented (Hirche and Mumm 1992, Mumm 1993).

In accordance with the hypothesis of a hydrographical pattern and previous studies, highest biomass values were found in the core of the Atlantic inflow (Kosobokova 2009), with decreasing AW influence biomass values decreased respectively. Smaller fractions dominated the biomass composition at the AR stations. A possible overestimation of the 1000-2000 μm size-fraction could be partially responsible for these results as shown below. Stations associated with the AW inflow on the shelf and slope (Rudels et al. 2015) show high biomasses compared to the Nansen Basin. It can be assumed that the AW influence is one of the driving factors, since stations located in the Nansen Basin, but influenced by AW showed differences compared to other stations in the Nansen Basin that were not influenced by AW.

The results show that there is a significant positive relationship between ZooScan-based biomass and dry weight biomass. Similar results were found in the South Yellow Sea (Dai et al. 2016), where results showed significant correlations between the biovolume and the dry mass, but insignificant for samples in size of 500-1000 μm and $>2000 \mu\text{m}$, due to the taxa composition.

Both methods show similar relative proportions but have their distinctive biases. In first instance I would have expected that the ZooScan-based method would rather underestimate biomass compared to the direct weighing method. However, the total biomass estimated with the ZooScan was almost twice as high as the dry weight-measured biomass. A comparison of the relationship between dry-weight biomass estimates and ZooScan-based biomass estimates showed that the bulk of this discrepancy was made up by differences in the total values of the 500-1000 μm and 1000-2000 μm size-fractions (Figure 21). Different conclusions were also made based on the data acquired by Zakharova (2019), who observed no significant differences between stations influenced by AW and polar-influenced waters. Also, stations in the Nansen Basin showed an average higher biomass than stations on the shelf and slope according to Zakharova (2019). My study however found the opposite pattern.

It could be assumed that one of the major reasons for scaling differences was the selection of conversion factors for the different taxa. When converting ZooScan-based biovolume into dry biomass that can be compared to the measured dry weight biomass, different conversion factors were selected for each taxon or group of taxa. Gelatinous zooplankton with high water content cannot be compared with, for example, crustacea and therefore various conversion factors are needed (Lehette and Hernández-León 2009).

Conversion factors used in this study were predominantly based on subtropical and Antarctic organisms (Lehette and Hernández-León 2009) and not from the Arctic. Although it was tried to use the conversion factors most suited for the particular Arctic species, certain deviations are probably unavoidable. For future research I recommend using conversion factors for the specific species. Regression and correlation parameters between body area and individual dry mass for these species will be needed. The usage of length-weight relationship would be ideal.

C. glacialis and *C. finmarchicus* were most prominent in the 500-2000 μm size-fractions with high abundances. Even a small deviation from the conversion factor can therefore lead to distinct differences in total biomass estimations. Both *Calanus* species were grouped together and used the same conversion factor of the Antarctic species *Calanus propinquus*. While the length of *C. propinquus* compares well with average lengths of *C. glacialis*, the smaller *C. finmarchicus* was overestimated with this conversion factor. Dry weight (μg) and length (mm) estimates of female adult *C. finmarchicus* (235 μg (Tande 1982, Tande and Slagstad 1992), 2.4-3.2 mm (Hirche et al. 1994)) and *C. glacialis* (600 μg (Hanssen 1997, Hirche and Kosobokova 2003), 3.2-4.6 mm (Hirche et al. 1994)) show distinct differences and some studies suggest differences in lipid mass for *C. finmarchicus* (0.08 mg ind^{-1} (Scott et al. 2000)) and *C. glacialis* (0.45 mg ind^{-1} (Scott et al. 2000)).

Assuming more *C. finmarchicus* than *C. glacialis* were present in the sampled areas of this study, it would lead to a general overestimation of the size-fraction and conversely to an underestimation if more *C. glacialis* than *C. finmarchicus* were present. A length distribution frequency analysis of both species in the study area was made by Klasmeier (2019) and higher dry weight biomass of *C. glacialis* (median of 1.42 mg m^{-2}) compared to *C. finmarchicus* (median of 1.28 mg m^{-2}) was found in the surface layer (0-2 m). Based on my results, which showed distinct differences in the 1000-2000 μm between dry weight measured biomass and ZooScan-based biomass it can be assumed that there is a potentially high error due to overestimation of the dry weight due to a high share of *C. finmarchicus* in the 500-2000 μm size classes. The usage of species-specific conversion factors could reduce the deviation between biovolume, and biomass estimates and lead to more realistic results. An adjustment for conversion factors of *Calanus glacialis* and *Calanus finmarchicus* could show reduced biomass estimates in the Atlantic inflow core for this study, possibly reducing the discrepancy with the results of Zakharova (2019).

Besides this aspect, several technical aspects of the ZooScan method bear the potential of additional but probably small method biases:

For the calculation of the dry weight biomass, all the samples were split in two halves in the study (Zakharova 2019). In contrast some of the largest samples had a split ratio of up to 1/256 to be prepared for the ZooScan, leading to potentially higher deviations. A Motoda plankton splitter was used to split the samples. When dividing into sub-samples, systematic or accidental division errors easily occur, because organisms have an uneven probability of splitting between the two subsamples (Sell and Evans 1982) or organisms could get jammed with each other. As a result, the Motoda plankton splitter was tilted at least 20-30 times to ensure even distribution. Division errors are more likely to occur when dividing the sample many times (Van Guelpen et al. 1982). This applies particularly to large samples. However, depending on the size of the organisms, the ZooScan can scan approximately 1000-1500 organisms at the same time (Gorsky et al. 2010), nevertheless given the size of the samples for this study, splitting ratio for most stations couldn't be kept low, possibly leading to random errors.

Organisms might be damaged or body parts such as antennas or legs may fall off due to transfer into different vessels or sieves. Above all, Appendicularia have been found particularly vulnerable in this study. This could lead to a misinterpreted biovolume. Even with undamaged organisms, antennas or legs may be covered by the rest of the body, depending on the individual's position. Therefore, fallen off body parts were not considered in the calculation of ZooScan-based biomass.

Several organisms in a sample can be determined relatively quickly with the ZooScan and the automatic prediction saves time with identification (Benfield 2007), given the availability of a good Learning Set prior. However more work steps are necessary, leading to potentially more systematic errors.

For the analysis with the ZooScan, the organisms which were previously contained in formaldehyde solution were rinsed with water and transferred to the sieves with different mesh sizes. The transfer had to be done very carefully. Small organisms, in particular, can get caught on the walls of the vessels, which required to rinse the vessels several times with water. When transferring the samples to sieves with different mesh sizes, a distinctive spread of the organisms was needed and required thoroughly rinsing once again. As a result, long but thin organisms, such as chaetognaths can easily slip into sieve with the next smaller mesh size. It is possible that the 1000 micrometer sieve acted as the major retention step for larger animals from higher size classes.

Another hypothesis was that Biomass could serve as proxy for community composition and abundance, which would facilitate gaining a quick overview over studied communities, despite the sheer number of unexamined samples.

There was a significant positive relationship between biomass and abundance ($R^2 = 0.89$), which could imply that biomass values can serve as proxy of mesozooplankton abundance in this study. The stations with highest biomass also compare well with the stations showing highest abundance.

Regarding community composition, predictions about the dominant Copepoda groups could be made. *C. glacialis* and *C. finmarchicus* together accounted for more than 90% in size class 500-1000 μm , therefore it could be assumed that high biomass values in this size class respectively correspond to a high abundance of these two species. Furthermore *C. hyperboreus* accounted for more than 60% in size class 2000-4000 μm . Stations with high biomass values of this size class could indicate abundances of *C. hyperboreus*.

However, the copepod community structure in the Arctic Ocean is influenced by various factors, such as regional and seasonal changes and variations in environmental factors. Assumptions based on biomass alone regarding community composition are not reliable without thorough understanding of the seasonal, regional and environmental context. But taxonomic analysis of reference samples could help to give context and acquire a general overview, without considering rare species. However, reference samples must be interpreted accordingly to the environmental factors and changes, such as hydrographical patterns.

This study confirmed the hypothesis that there was a biogeographical and more importantly hydrographical pattern of mesozooplankton community structure in the study area of PS106. Biomass and abundance were highest along stations in the AR and lowest at stations in the PR. Smaller size-fractions with high abundances dominated the AR and larger size fractions the PR respectively. Growing AW influences can therefore have consequences for the ecosystem structure and the sustainability for marine resources, such as commercially used fish and the characteristic megafauna.

It was shown that a more traditional method for calculating biomass such as a dry weight measurement leads to similar relative proportions as ZooScan-based biomass, which would allow for a more rapid taxonomic analysis and biomass calculation of the vast number of samples. It can be assumed that the algorithm for automatic prediction will continue to improve, as well as scanning technology, leaving a lot of future potential for the ZooScan method (Gorsky et al. 2010, Wickline 2016). Regression and correlation parameters between body area and individual dry mass for the analyzed species and the usage of length-weight relationship, however are essential to improve accuracy of the ZooScan method.

Finally, there was a link between high biomasses and high abundances, which would enable faster predictions based on biomass alone in well-studied ecosystems. It can be assumed that climate change will bring more AW to the regions (Zhang et al. 1998, Ślubowska et al. 2005), therefore further influencing the community compositions in the regions. The results of this thesis show, in agreement with previous studies, that an increased Atlantic influence is probably associated with more abundant but smaller mesozooplankton species in the study region.

5 Literature

- Aksenov P.V., Ivanov V.V. (2018) “Atlantification” as a possible cause for reducing of the sea-ice cover in the Nansen Basin in winter. *Arctic and Antarctic Research* 64(1): 42-54. doi:10.30758/0555-2648-2018-64-1-42-54
- Årthun M., Eldevik T., Smedsrud L.H., Skagseth Ø. , Ingvaldsen R.B. (2012) Quantifying the influence of Atlantic heat on Barents Sea ice variability and retreat. *Journal of Climate* 25, 4736–4743. doi:10.1175/JCLI-D-11-00466.1
- Bell J.L., Hopcroft R.R. (2008) Assessment of ZooImage as a tool for the classification of zooplankton. *Journal of Plankton Research* 30:1351–1367. doi:10.1093/plankt/fbn092
- Benfield M.C., P. Grosjean, P.F. Culverhouse, X. Irigoien, M.E. Sieracki, A. Lopez-Urrutia, H.G. Dam, Q. Hu, C.S. Davis, A. Hansen, C.H. Pilskaln, E.M. Riseman, H. Schultz, P.E. Utgoff, and G. Gorsky (2007) RAPID: Research on Automated Plankton Identification. *Journal of Oceanography* 20(2):172–187, doi:10.5670/oceanog.2007.63.
- Blachowiak-Samolyk K., Søreide J.E., Kwasniewski S., Sundfjord A., Hop H., Falk-Petersen S., Nøst Hegseth E. (2008) Hydrodynamic control of mesozooplankton abundance and biomass in northern Svalbard waters (79–81°N). *Deep Sea Research Part II Top Studies Oceanography* 55:2210–2224. doi:10.1016/J.DSR2.2008.05.018
- Bluhm B.A., Kosobokova K.N., Carmack E.C. (2015) A tale of two basins: An integrated physical and biological perspective of the deep Arctic Ocean. *Progress in Oceanography*, Volume 139, Pages 89-121. doi:10.1016/j.pcean.2015.07.011.
- Bray J.R., Curtis J.T. (1957) An Ordination of the Upland Forest Communities of Southern Wisconsin. *Ecological Monographs* 27(4): 326-349.
- Carmack E.C. (2000) The Arctic Ocean’s freshwater budget: Sources, storage and export. In *The freshwater budget of the Arctic Ocean*, eds. E.L. Lewis, P.E. Jones, P. Lemke, T.D. Prowse and P. Wadhams, 91–126. The Netherlands: Kluwer Academic Press.
- Castellani G., Flores H. Lange B.A., Schaafsma F.L., Ehrlich J., David C.L., van Franeker J.A., Meijboom A., van Dorssen M., Vortkamp M., Van de Putte A. (2019) Sensor data from SUIT measurements during POLARSTERN cruise PS106. PANGAEA. doi:10.1594/PANGAEA.902283 (dataset in review),
- Daase M., Eiane K. (2007) Mesozooplankton distribution in northern Svalbard waters in relation to hydrography. *Polar Biology* 30(8): 969-981.

- Daase M., Kosobokova K., Last K.S., Cohen J.H., Choquet M., Hatlebakk M., Søreide J.E. (2018) New insights into the biology of *Calanus* spp. (Copepoda) males in the Arctic. *Marine Ecology Progress Series* 607:53-69. doi:10.3354/meps12788
- Dai L.P., Li C.L., Wang S.W., Wang Y.Q., Zhang F. (2016) Analysis of community structure of zooplankton in South Yellow Sea in summer with ZooScan. *Oceanologia et Limnologia Sinica*, 47(4): 764-773. doi:10.11693/hyhz20160200029
- David C., Lange B., Rabe B., Flores H. (2015) Community structure of under-ice fauna in the Eurasian central Arctic Ocean in relation to environmental properties of sea-ice habitats. *Marine Ecology Progress Series*, 522, 15-32.
- Falk-Petersen S., Mayzaud P., Kattner G., Sargent J.R. (2009) Lipids and life strategy of Arctic *Calanus*. *Marine Biology Research* 5(1): 18-39.
- Finkel Z., Beardall J., Flynn K.J., Quigg A., Alwyn T., Rees V., Raven J.A. (2010) Phytoplankton in a changing world: cell size and elemental stoichiometry. *Journal of Plankton Research*, Volume 32, Issue 1, January 2010, Pages 119–137. doi:10.1093/plankt/fbp098
- Flores H., Julia Ehrlich J., Lange B., Erik Sulanke E., Niehoff B., Hildebrand N., Doble M.; Schaafsma F., Meijboom A., Fey B., Kühn S., Bravo-Rebolledo E., van Dorssen M., Gradinger R., Hasset B., Kunisch E., Kohlbach D., Graeve M., van Franeker J., Bluhm B. (2018) Under-ice fauna, zooplankton and endotherms (In: Macke A. & Flores H. (2018) *The Expeditions PS106/1 and 2 of the Research Vessel POLARSTERN to the Arctic Ocean in 2017, Berichte zur Polar- und Meeresforschung = Reports on polar and marine research*) Bremerhaven, Alfred Wegener Institute for Polar and Marine Research, 719, 123-133, doi:10.2312/BzPM_0719_2018
- Fossheim M., Primicerio R., Johannesen E., Ingvaldsen R.B. Aschan M.M., Dolgov A.V., (2015) Recent warming leads to a rapid borealization of fish communities in the Arctic. *Nature Climate Change* 5, 673–677. doi:10.1038/nclimate2647.
- Giering S.L.C., Wells S., Mayers K.M.J, Schuster H., Cornwell L., Fileman E.S., Atkinson A., Cook K.B., Preece C., Mayor D.J. (2019) Seasonal variation of zooplankton community structure and trophic position in the Celtic Sea: A stable isotope and biovolume spectrum approach. *Progress in Oceanography*, Volume 177. doi:10.1016/j.pocean.2018.03.012.

- Gislason A., Silva T. (2009) Comparison between automated analysis of zooplankton using ZooImage and traditional methodology. *Journal of Plankton Research* 31:1505–1516.
doi:10.1093/plankt/fbp094
- Gorsky G., Ohman M.D., Picheral M., Gasparini S., Stemmann L., Romagnan J.B., Cawood A., Pesant S., García-Comas C., Prejger F. (2010) Digital zooplankton image analysis using the ZooScan integrated system. *Journal of Plankton Research* 32:285–303.
doi:10.1093/plankt/fbp124
- Grosjean P., Picheral M., Warembourg C., Gorsky G. (2004) Enumeration, measurement, and identification of net zooplankton samples using the ZOOSCAN digital imaging system. *ICES Journal of Marine Science* 61:518–525. doi:10.1016/j.icesjms.2004.03.012
- Hanssen H. (1997) Mesozooplankton of the Laptev Sea and the adjacent eastern Nansen Basin—distribution and community structure in late summer. *Berichte zur Polarforschung*, 229: 1–131.
- Hays G.C., Richardson A.J., Robinson C. (2005) Climate change and marine plankton. *Trends in Ecology & Evolution* 20:337–344. doi:10.1016/j.tree.2005.03.004
- Hays G.C., Richardson A.J., Robinson C. (2005) Climate change and marine plankton. *Trends in Ecology & Evolution* 20(6): 337-344.
- Hernández-León S., Montero I. (2006) Zooplankton biomass estimated from digitalized images in Antarctic waters: A calibration exercise. *Journal of Geophysical Research* 111, C05S03, doi:10.1029/2005JC002887.
- Hirche H.J., Hagen W., Mumm N. et al. (1994) The Northeast Water polynya, Greenland Sea. *Polar Biol* 14, 491–503. doi:10.1007/BF00239054
- Hirche H.J., Kosobokova K.N. (2003) Early reproduction and development of dominant calanoid copepods in the sea ice zone of the Barents Sea—need for a change of paradigms? *Marine Biology*, 143: 769–781.
- Hirche H.J., Kosobokova K.N. (2011) Winter studies on zooplankton in Arctic seas: the Storfjord (Svalbard) and adjacent ice-covered Barents Sea. *Marine Biology* 158, 2359–2376
doi:10.1007/s00227-011-1740-5

Hirche H.J., Mumm N. (1992) Distribution of dominant copepods in the Nansen Basin, Arctic Ocean, in summer. *Deep-Sea Res* 39 [Suppl 2]:S485±S505

Jakobsson M., Grantz A., Kristoffersen Y., Macnab R. (2003) Physiographic provinces of the Arctic Ocean seafloor. *GSA Bulletin*; 115 (12): 1443–1455. doi:10.1130/B25216.1

Jakobsson M., Grantz A., Kristoffersen Y., Macnab R. (2004) The Arctic Ocean: Boundary conditions and background information. In *The organic carbon cycle in the Arctic Ocean*, eds. R. Stein and R.W. Macdonald, 1– 32. Berlin: Springer-Verlag.

Jakobsson M., Macnab R., Mayer L., Anderson R., Edwards M., Hatzky J., Schenke H.W., Johnson P. (2008) An improved bathymetric portrayal of the Arctic Ocean: Implications for ocean modeling and geological, geophysical and oceanographic analyses. *Geophysical Research Letters* 35: L07602.

Kortsch S., Primicerio R., Fossheim M., Dolgov A.V., Aschan M. (2015) Climate change alters the structure of arctic marine food webs due to poleward shifts of boreal generalists. *Proceedings of the Royal Society B: Biological Sciences* 282. doi:10.1098/rspb.2015.1546. pii: 20151546.

Kosobokova K.N. (1982) Composition and distribution of the biomass of zooplankton in the central Arctic Basin. *Oceanology* 22:744±750

Kosobokova K.N., Hirche H.J. (2009) Biomass of zooplankton in the eastern Arctic Ocean—a base line study. *Progress in Oceanography*, 82(4), 265-280.

Lehette P., Hernández-León S. (2009) Zooplankton biomass estimation from digitized images: a comparison between subtropical and Antarctic organisms. *Limnology and Oceanography: Methods*, 7, doi:10.4319/lom.2009.7.304.

Loeng H. (1991) Features of the physical oceanographic conditions of the Barents Sea, *Polar Research*, 10:1, 5-18, doi:10.3402/polar.v10i1.6723

Matsuno K., Yamaguchi A., Shimada K., Imai I. (2012) Horizontal distribution of calanoid copepods in the western Arctic Ocean during the summer of 2008. *Polar Science*, Volume 6, Issue 1, Pages 105-119. doi:10.1016/j.polar.2012.01.002.

Michel C., Bluhm B., Gallucci V., Gaston A.J., Gordillo F.J.L., Gradinger R., Hopcroft R., Jensen N., Mustonen T., Niemi A., Nielsen T.G. (2012) Biodiversity of Arctic marine ecosystems and responses to climate change, *Biodiversity*, 13:3-4, 200-214.
doi:10.1080/14888386.2012.724048

Motoda S. (1959) Devices of simple plankton apparatus. *Memoirs of the Faculty of Fisheries Hokkaido University*, 7(1-2), 73-94.

Mumm N. (1993) Composition and distribution of mesozooplankton in the Nansen Basin, Arctic Ocean, during summer. *Polar Biology*, 13(7), 451-461

Zakharova N. (2019). Trophic structure and biomass of high-Arctic zooplankton in the Eurasian Basin in 2017. Master Thesis. Saint Petersburg State University / Hamburg University

Nicolopoulos A., Heuze C., Linders T., Andree E., Sahlin A. (2018) Physical Oceanography (In: Macke A. and Flores H. (2018): *The Expeditions PS106/1 and 2 of the Research Vessel POLARSTERN to the Arctic Ocean in 2017*, *Berichte zur Polar- und Meeresforschung = Reports on polar and marine research*) Bremerhaven, Alfred Wegener Institute for Polar and Marine Research, 719, 123-133, doi:10.2312/BzPM_0719_2018.

Oksanen J., Guillaume Blanchet F., Friendly M., Kindt R., Legendre P., McGlinn D., Minchin P.R., O'Hara R. B., Simpson G.L., Solymos P., Henry M., Stevens H., Szoecs E., Wagner H. (2013) Package 'vegan'. *Community Ecology Package*

Picheral M., Colin S., Irisson J.O. (2017) EcoTaxa, a tool for the taxonomic classification of images. <http://ecotaxa.obs-vlfr.fr>.

Pidwirny M. (2006) Introduction to the Oceans. *Fundamentals of Physical Geography*, www.physicalgeography.net, 2nd Edn. Ch. 8.
<http://www.physicalgeography.net/fundamentals/8o.html>

Pielou E. C. (1969) *An Introduction to Mathematical Ecology*. John Wiley.

Roe H. and Shale D. (1979) A new multiple rectangular midwater trawl (RMT 1+8M) and some modifications to the Institute of Oceanographic Sciences' RMT 1+8. *Marine Biology* 50, 283-288.

- Roe H.S.J., Baker A.d.C., Carson R.M. et al. (1980) Behaviour of the institute of oceanographic science's rectangular midwater trawls: Theoretical aspects and experimental observations. *Marine Biology* 56, 247–259 (1980). doi:10.1007/BF00645349
- Rolke M., Lenz J. (1984) Size structure analysis of zooplankton samples by means of an automated image analyzing system. *Journal of Plankton Research* 6:637–645. doi:10.1093/plankt/6.4.637
- Rudels B., Schauer U., Björk G., Korhonen M., Pisarev S., Rabe B., Wisotzki A. (2013) Observations of water masses and circulation in the Eurasian Basin of the Arctic Ocean from the 1990s to the late 2000s. OS Special Issue: Ice-Atmosphere-Ocean interactions in the Arctic Ocean during IPY: the Damocles project, 9 (1), pp. 147-169 . doi:10.5194/os-9-147-2013
- Rudels B., Jones E., Anderson L., Kattner G. (1994) On the intermediate depth waters of the Arctic Ocean. *The polar oceans and their role in shaping the global environment*, 85, 33-46.
- Sakshaug E. (2004) Primary and Secondary Production in the Arctic Seas. Stein R., MacDonald R.W. (eds) *The Organic Carbon Cycle in the Arctic Ocean*. Springer, Berlin, Heidelberg. doi:10.1007/978-3-642-18912-8_3
- Schauer U., Muench R., Rudels B., Timokhov L. (1997) Impact of eastern Arctic shelf waters on the Nansen Basin intermediate layers. *Journal of Geophysical Research: Oceans*, 102(PR), 33713382.
- Scott C., Kwasniewski S., Falk-Petersen S. et al. (2000) Lipids and life strategies of *Calanus finmarchicus*, *Calanus glacialis* and *Calanus hyperboreus* in late autumn, Kongsfjorden, Svalbard. *Polar Biol* 23, 510–516. doi:10.1007/s003000000114
- Sell D.W., Evans M.S. (1982) A statistical analysis of subsampling and an evaluation of the Folsom plankton splitter. *Hydrobiologia* 94:223–230. doi:10.1007/BF00016403
- Shannon C.E., Weaver W. (1949) *The mathematical theory of communication*. The University of Illinois. Urbana, Chicago, London. pp. 3–24.
- Ślubowska M. A., Koç N., Rasmussen T. L., Klitgaard-Kristensen D. (2005) Changes in the flow of Atlantic water into the Arctic Ocean since the last deglaciation: Evidence from the northern Svalbard continental margin, 80°N, *Paleoceanography*, 20, PA4014, doi:10.1029/2005PA001141.

Sundfjord A., Fer I., Kasajima Y., Svendsen H. (2007) Observations of turbulent mixing and hydrography in the marginal ice zone of the Barents Sea. *Journal of Geophysical Research* 112, C05008, doi:10.1029/2006JC003524.

Tande K. S. (1982). Ecological investigations on the zooplankton community of Balsfjorden, northern Norway: Generation cycles, and variations in body weight and body content of carbon and nitrogen related to overwintering and reproduction in the copepod *Calanus finmarchicus* (Gunnerus). *Journal of Experimental Marine Biology and Ecology*, 62: 129–142.

Tande K. S., Slagstad D. (1992) Regional and interannual variations in biomass and productivity of the marine copepod, *Calanus finmarchicus*, in sub-arctic environments. *Oceanologica Acta*, 15: 309–321.

Thibault D., Head E.J.H., Wheeler P.A. (1998) Mesozooplankton in the Arctic Ocean in summer. *Deep Sea Research Part I: Oceanographic Research Papers* 46(8): 1391-1415.

Vandromme P., Stemmann L., Garcia-Comas C., Berline L., Sun X., Gorsky G. (2012) Assessing biases in computing size spectra of automatically classified zooplankton from imaging systems: A case study with the ZooScan integrated system. *Methods in Oceanography*, Volumes 1–2, Pages 3-21. doi:10.1016/j.mio.2012.06.001.

Van Guelpen L., Markle D.F., Duggan D.J. (1982) An evaluation of accuracy, precision, and speed of several zooplankton subsampling techniques. *ICES Journal of Marine Science* 40:226–236. doi:10.1093/icesjms/40.3.226

Vinje T., Kvambekk Å.S. (1991) Barents Sea drift ice characteristics*. *Polar Research*, 10: 59-68. doi:10.1111/j.1751-8369.1991.tb00635.x

Wassmann P., Reigstad M., Haug T., Rudels B., Carroll M.L., Hop H., Gabrielsen G.W., Falk-Petersen S., Denisenko S.G, Arashkevich E., Slagstad D., Pavlova O. (2006) Food webs and carbon flux in the Barents Sea. *Progress in Oceanography*. 71. doi:10.1016/j.pocean.2006.10.003

Wickline A. (2016) Seasonal and historical mesozooplankton dynamics in Delaware Bay: an application and optimization of the ZooScan optical imaging tool. Master Thesis. University of Delaware. <http://udspace.udel.edu/handle/19716/20458>

Wilcoxon F. (1945) Individual Comparisons by Ranking Methods. *Biometrics Bulletin* 1(6): 80-83. doi:10.2307/3001968

Zhang J., Rothrock D.A., Steele M. (1998) Warming of the Arctic Ocean by a strengthened Atlantic Inflow: Model results. *Geophysical Research Letters* 25. doi:10.1029/98GL01299

6 Appendix

Table A. 1: Taxonomic composition and abundance of mesozooplankton across the Barents Sea shelf slope and Nansen Basin for the Atlantic regime Cluster (AR)

	Station	52	64	65	67	70	78	80	83
Family	Species/Taxa	27	23	20	18	17	18	18	21
Acartiidae	<i>Acartia</i>	0.05							
Calanidae	<i>C. finmarchicus/glacialis</i>	64.07	27.62	18.59	23.12	39.78	37.17	139.88	47.15
	<i>Calanus hyperboreus</i>	3.25	0.66	1.25	2.37	8.29	2.56	3.13	1.11
Actideidae	<i>Chiridius obtusifrons</i>				<0.01				
Heterorhabdidae	<i>Heterorhabdus norvegicus</i>			0.06	0.14	0.40	0.31		
Metridinidae	<i>Metridia longa</i>	1.91	2.61	0.06	5.58	8.26	10.26	37.06	1.88
Clausocalanidae	<i>Microcalanus</i>	0.03			<0.01			0.13	0.05
Euchaetidae	<i>Paraeuchaeta</i>	0.23	0.33	0.66	2.36	0.64	1.01	0.65	0.52
Clausocalanidae	<i>Pseudocalanus</i>	18.44	1.24	0.87	0.86	0.73	0.54	14.52	2.11
Scolecitrichidae	<i>Scolecitrichella minor</i>	0.11	0.05	0.06	0.45	0.07	0.23		0.05
	Unidentified Calanoida	0.11	0.11	0.06	0.14	0.22		0.59	0.10
Oithonidae		1.48	0.78	0.94	2.61	0.12	1.51	4.23	2.12
Oncaidae									
Ectinosomatidae	<i>Microsetella</i>								0.01
Mormonillidae									
	Unidentified Copepoda (badfocus)	1.08	0.44	1.29	1.05	0.40	0.75	2.28	0.68
	Foraminifera	0.03	0.01	0.03			0.01	0.03	0.07
	Hydrozoa, Scyphozoa	0.62	0.13	0.44			0.35		
	Siphonophorae	<0.01	<0.01						0.10
	Bivalvia	<0.01							
Clionidae	<i>Clione limacina</i>	0.02	0.14						
	Unidentified Gastropoda	0.18	0.02	0.03		<0.01	0.08		
	Polychaeta larvae	<0.01	0.04						
	Trochophore larvae	0.05	0.08						
	Amphipoda	0.46	0.04	1.61	1.58	5.13	4.63	1.76	0.45
	Euphausiacea Juvenile/adult	0.25	0.05	0.14	0.2	0.25	0.14	0.02	0.01
	Euphausiacea Furcilia stages							0.52	0.01
	Euphausiacea Calytopis stages							1.07	0.16
	Isopoda	0.11	0.04	0.06	0.05	0.02	0.01		
	Ostracoda	0.03	0.01	0.06	0.23	0.09	1	1.17	0.05
	Unidentified nauplii (mostly Copepoda)	0.22	0.16	0.07			0.08	1.24	0.7
	Chaetognatha	0.88	0.60	0.56	1.07	2.41	0.98	6.61	1.34
	Appendicularia	0.46	0.03	0.27	0.09	0.66	0.17	1.2	0.75
	Pisces larvae	0.03							

Table A. 2: Taxonomic composition and abundance of mesozooplankton across the Barents Sea shelf slope and Nansen Basin for the polar regime Cluster (PR)

Station	71	72	73	74	75	76	77	
Family	Species/Taxa	19	16	17	17	19	17	18
Acartiidae	<i>Acartia</i>							
Calanidae	<i>C. finmarchicus/glacialis</i>	13.52	8.05	4.57	5.45	9.15	1.22	10.31
	<i>Calanus hyperboreus</i>	3.44	6.00	2.18	4.35	5.54	2.34	3.31
Aetideidae	<i>Chiridius obtusifrons</i>		0.10					
Heterorhabdidae	<i>Heterorhabdus norvegicus</i>	0.09				0.01	<0.01	
Metridinidae	<i>Metridia longa</i>	3.17	2.02	2.66	3.74	8.24	3.75	2.24
Clausocalanidae	<i>Microcalanus</i>	<0.01				0.04		
Euchaetidae	<i>Paraeuchaeta</i>	1.08	0.66	0.69	0.66	0.29	0.12	0.48
Clausocalanidae	<i>Pseudocalanus</i>	0.3	0.36	0.19	0.08	0.2		0.58
Scolecitrichidae	<i>Scolecitrichella minor</i>	0.21	0.10	0.06	0.20		0.03	
	Unidentified Calanoida				0.08	0.08	0.03	0.12
Oithonidae		1.84	1.29	0.82	2.14	2.40	1.23	0.40
Oncaeidae					<0.01		0.01	
Ectinosomatidae	<i>Microsetella</i>							
Mormonillidae				0.01				
	Unidentified Copepoda (badfocus)	0.62	0.73	0.59	0.56	0.73	0.44	0.79
	Foraminifera	0.02				0.08	0.05	
	Hydrozoa, Scyphozoa	0.07			0.16	0.01	0.17	0.07
	Siphonophorae							
	Bivalvia							
Clionidae	<i>Clione limacina</i>							
	Unidentified Gastropoda	0.05	0.05	0.06	0.12		0.03	0.01
	Polychaeta larvae							
	Trochophore larvae							
	Amphipoda	2.06	1.01	0.71	1.12	2.25	0.67	2.46
	Euphausiacea Juvenile/adult	0.05		0.04		0.05		0.26
	Euphausiacea Furcilia stages							
	Euphausiacea Calyptopsis stages							0.06
	Isopoda	0.07	0.10	0.12	0.10	0.35	0.11	0.2
	Ostracoda	0.02	0.16	0.01		0.08		0.13
	Unidentified nauplii (mostly Copepoda)		0.21	0.06	0.17	0.20	0.18	0.22
	Chaetognatha	1.56	1.28	0.83	0.59	1.00	0.30	1.50
	Appendicularia	0.98	1.51	1.41	3.47	1.02	2.29	2.13
	Pisces larvae							

Table A. 3: Summary of statistical evaluation (n = sample size, W = Wilcoxon statistical criterion, p -value)

Parameter	n	W	p
Abundance of Mesozooplankton			
PR	7	30	0.001243
AR	8		
Diversity Index			
PR	7	36	0.000311
AR	8		
Total amount of Taxa			
PR	7	37	0.028904
AR	8		
Total Biomass of Mesozooplankton			
PR	7	35	0.013986
AR	8		
Abundance of Copepods			
PR	7	30	0.001243
AR	8		
Abundance of non-copepods			
PR	7	58	0.53582
AR	8		
Abundance Chaetognatha			
PR	7	52	0.694328
AR	8		
Abundance Appendicularia			
PR	7	38	0.001243
AR	8		
Relative abundance of <i>C. finm./glac.</i>			
PR	7	28	0.000311
AR	8		
Relative abundance of <i>C. hyperboreus</i>			
PR	7	36	0.000311
AR	8		

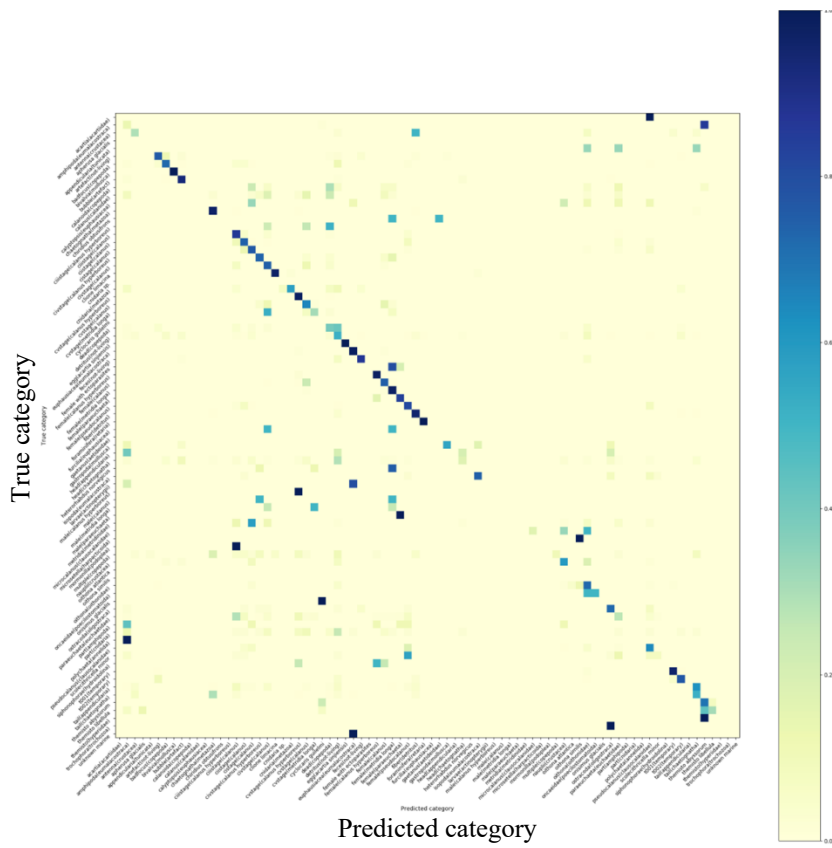


Figure A. 1: Confusion matrix from EcoTaxa, diagonal contains the recall rate, darker blue indicates a higher rate. For all categories see Tab. A.3.

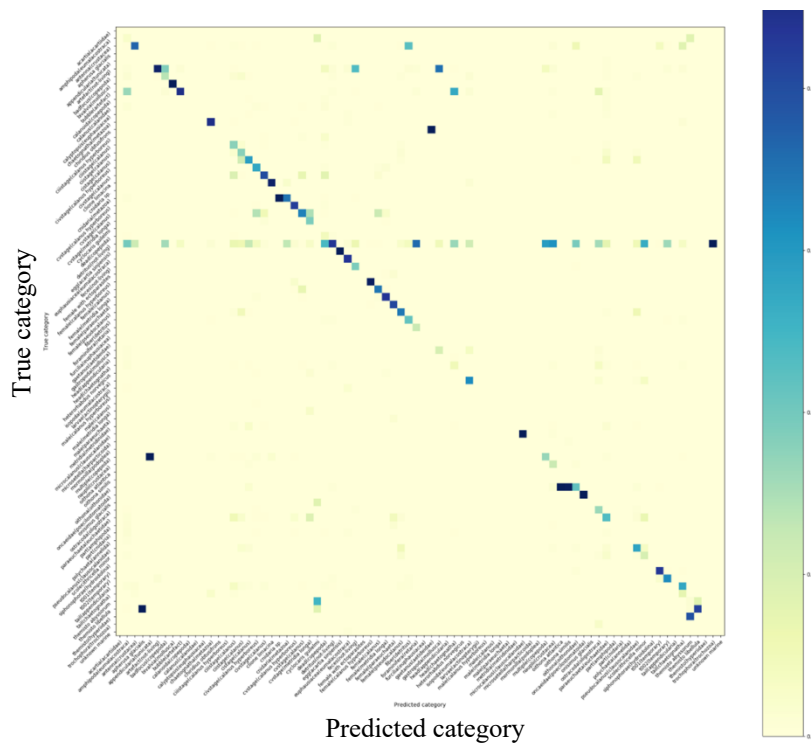


Figure A. 2: Confusion matrix from EcoTaxa, diagonal contains the precision rate, darker blue indicates a higher rate. For all categories see Tab. A.3.

Table A. 4: All categories of the learning set in EcoTaxa

acartia (acartiidae)	furcilia (euphausiacea)
amphipoda (eumalacostraca)	gaetanus (aetideidae)
antenna (crustacea)	gastropoda (mollusca)
apherusa glacialis	head (appendicularia)
appendicularia (tunicata)	head (chaetognatha)
artefact (not-living)	heterohabdus norvegicus
badfocus (copepoda)	isopoda (eumalacostraca)
bivalvia (mollusca)	larvae (actinopterygii)
bubble (artefact)	male (calanus hyperboreus)
calanoida (copepoda)	male (calanus)
calanus (calanidae)	male (metridia longa)
calyptopsis (euphausiacea)	male (paraeuchaeta)
chaetognatha (metazoa)	metridia (metridinidae)
chiridius obtusifrons	microcalanus (clausocalanidae)
ciistage (calanus hyperboreus)	microsetella (harpacticoida)
ciistage (calanus)	mormonilla (podoplea)
ciistage (calanus)	multiple (copepoda)
cistage (calanus)	nauplii (crustacea)
civstage (calanus hyperboreus)	oithona atlantica
civstage (calanus)	oithona similis
clione limacina	oithona (oithonidae)
cnidaria sp.	oncaeidae (poecilostomatoida)
cnidaria (metazoa)	onisimus glacialis
cvstage (calanus hyperboreus)	ostracoda (oligostraca)
cvstage (calanus)	paraeuchaeta (euchaetidae)
cvstage (metridia longa)	part (amphipoda)
cyclocaris guilelmi	part (cnidaria)
dead (copepoda)	polychaeta (annelida)
detritus (not-living)	pseudocalanus (clausocalanidae)
egg (acartia sinjiensis)	scolecithricella minor
euphausiacea (eumalacostraca)	siphonophorae (hydroidolinan)
feces (not-living)	t001 (temporary)
female with ectoparasites	t002 (temporary)
female (calanus hyperboreus)	tail (appendicularia)
female (calanus)	tail (chaetognatha)
female (metridia longa)	themisto abyssorum
female (paraeuchaeta)	themisto libellula
female (pseudocalanus)	themisto (hyperiididae)
fiber (detritus)	trochophore (trochozoa)
foraminifera (retaria)	unknown marine

7 Acknowledgements

First and foremost, I would like to thank my supervisor, Dr. Hauke Flores, for always keeping me motivated with his humor and sharing his insightful experience. I'm also grateful that he gave me the opportunity of writing my thesis at the Alfred Wegener Institute in Bremerhaven.

Furthermore, I would like to thank Dr. Jens Floeter, who agreed to act as my second supervisor and gave me helpful feedback whenever I asked. I would like to give special acknowledgment to Dr. Astrid Cornils for her guidance through each stage of the process, reviewing my thesis and answering all my questions. I would also like to thank everyone who I have met at Alfred Wegener Institute and who have welcomed me with open arms, curiously asking about my progress and giving me interesting insights.

Finally, I would like to thank my family and all my friends who offered emotional support and helped me through this exciting time.

Declaration of Academic Honesty

Hiermit erkläre ich an Eides statt, dass die vorliegende Arbeit von mir selbständig verfasst wurde und ich keine anderen als die angegebenen Hilfsmittel – insbesondere keine im Quellenverzeichnis nicht benannten Internet-Quellen – benutzt habe und die Arbeit von mir vorher nicht einem anderen Prüfungsverfahren eingereicht wurde. Die eingereichte schriftliche Fassung entspricht der auf dem elektronischen Speichermedium. Ich bin damit einverstanden, dass die Bachelorarbeit veröffentlicht wird

Hamburg, 25th April 2020

